Article

Not peer-reviewed version

TvAtg4.4 Autophagin Processes TvAtg8 Autophagy Proteins and Responds to Glucose in *Trichomonas vaginalis*

Miriam Guadalupe Mateo-Cruz , Claudia Ivonne Flores-Pucheta , Jaime Ortega-López , Lizbeth Iliana Salazar-Villatoro , Martha Espinosa-Cantellano , Rossana Arroyo *

Posted Date: 27 November 2025

doi: 10.20944/preprints202511.2032.v1

Keywords: autophagin; ATG8 autophagy marker proteins; cysteine protease; macroautophagy; TvAtg4.4 characterization; TvAtg8aGST; TvAtg8bGST; *Trichomonas vaginalis*

Article

TvAtg4.4 Autophagin Processes TvAtg8 Autophagy Proteins and Responds to Glucose in *Trichomonas vaginalis*

Miriam Guadalupe Mateo-Cruz [1], Claudia Ivonne Flores-Pucheta [2], Jaime Ortega-López [2], Lizbeth Ileana Salazar-Villatoro [1], Martha Espinosa-Cantellano [1] and Rossana Arroyo [1,*]

[1] Department of Infectomics and Molecular Pathogenesis, Center for Research and Advanced Studies of the National Polytechnic Institute (Cinvestav), Av. IPN 2508, Gustavo A. Madero (GAM), Mexico City 07360, Mexico

[2] Department of Biotechnology and Bioengineering, Center for Research and Advanced Studies of the National Polytechnic Institute (Cinvestav), Av. IPN 2508, Gustavo A. Madero (GAM), Mexico City 07360, Mexico

* Correspondence: rarroyo@cinvestav.mx; Tel: +52 55 5747 3342

Abstract

Microautophagy is a conserved cellular degradation process involving ATG proteins, with ATG4 proteases essential for processing ATG8 family proteins during autophagosome formation. In *Trichomonas vaginalis*, the role of autophagin proteases in processing autophagy markers TvAtg8a and TvAtg8b has not been fully characterized. In this study, we expressed and purified recombinant TvAtg4.4 and demonstrated its cysteine protease activity *in vitro*. TvAtg4.4 rapidly processed TvAtg8aGST and, to a lesser extent, TvAtg8bGST. Enzymatic assays confirmed substrate specificity and inhibition by cysteine protease inhibitors. TvAtg4.4 mRNA expression increased under glucose restriction, and immunolocalization showed its presence in autophagic vesicles, cytoplasm, endoplasmic reticulum, Golgi, lysosomes, hydrogenosomes, and nucleus. Colocalization with TvAtg8a and TvAtg8b supports its functional role in autophagy. The localization of TvAtg4.4 in autophagosomes and ER suggests its involvement in the cleavage of TvAtg8a and TvAtg8b after synthesis and in the delipidation or deconjugation of these proteins from the autophagosome outer membrane before autophagosome-lysosome fusion. These findings clarify the enzymatic function and cellular localization of TvAtg4.4, provide insight into autophagy mechanisms in *T. vaginalis*, and suggest potential novel roles for this protease in parasite biology.

Keywords: autophagin; ATG8 autophagy marker proteins; cysteine protease; macroautophagy; TvAtg4.4 characterization; TvAtg8aGST; TvAtg8bGST; *Trichomonas vaginalis*

1. Introduction

Macroautophagy is a self-digestive process that maintains cellular homeostasis by removing unnecessary or dysfunctional components through a lysosome-mediated mechanism. Macroautophagy is activated under stress conditions, such as nutrient deprivation, infection, and hypoxia. It is characterized by the formation of double-membrane vesicles called autophagosomes that surround the cargo (damaged organelles, protein aggregates, or cytoplasmic material) and then fuse with lysosomes to degrade its contents [1,2]. At the molecular level, the process follows five key stages: (1) Autophagy induction; (2) phagophore nucleation; (3) elongation of the phagophore; (4) autophagosome generation, and (5) autophagolysosome formation, where cargo proteins are degraded by lysosomal hydrolases. A set of genes encoding the "core" molecular machinery of macroautophagy, called ATG proteins, has been identified [3–5]. To date, 31 central *atg* genes have been transcribed and translated into ATG proteins, organized into five subgroups: (1) ULK complex,

 doi:10.20944/preprints202511.2032.v1

a serine/threonine kinase complex that responds to signals like nutrient deprivation to start autophagy; (2) Class lll Ptdlns3K complex, responsible for initiating the phagophore formation by generating phosphatidylinositol-3-phosphate (PtdIns3P) that helps recruit other ATG proteins, including (3) the WIPI/ATG18-ATG2 complex, involved in phagophore expansion and closure, and (4) two membrane proteins, ATG9/mAtg9 and VMP1, that provide membrane to the forming phagophore; and (5) two ubiquitin-like protein conjugation systems (Ubl) (ATG12 and ATG8/LC3) that are critical for phagophore elongation, and the formation and expansion of the autophagosome, respectively [6,7]. As the work is focused on this fifth subgroup, a more detailed description of the processes involved is presented.

The two ubiquitin-like conjugation systems include the Ubl proteins (ATG12 and ATG8/LC3), an activating enzyme (ATG7), two ubiquitin-conjugating enzyme analogues (ATG10 and ATG3), an ATG8/LC3-modifying protease (ATG4), the ATG12-binding protein (ATG5), and ATG16 [8]. These conjugation systems are widely conserved in eukaryotes and have essential roles. Specifically, the ATG8 conjugation system is involved in membrane elongation, cargo protein recognition, autophagosome closure, autophagosome trafficking, autophagosome-lysosome fusion, and inner membrane degradation [9]. However, lipidation of the ATG8/LC3 protein is necessary to perform its functions, for which the C-terminal end of ATG8/LC3 is cleaved by an ATG4 protease of the C54 family of autophagins to expose a glycine residue (Gly) to which a phosphatidylethanolamine (PE) is added, which enables the binding to the phagophore membranes to form autophagosomes. To allow the fusion of the autophagosome with the lysosome, the PE binding is known to be reversible, as the ATG4 protease, in a second event, removes the ATG8/LC3-PE bound to the outer membrane of the autophagosome, leaving again a Gly-exposed ATG8/LC3 [10,11].

Trichomonas vaginalis is the causative agent of trichomoniasis, the most common non-viral sexually transmitted infection (STI) worldwide, with more than 275 million cases annually [12]. In women, the infection manifests mainly with foamy, foul-smelling, greenish-yellow vaginal discharge. It is accompanied by pruritus, vulvar irritation, abdominal pain, edema, and a slight increase in vaginal pH (≥ 5.0). In severe cases, it has been linked to cervical neoplasia and pelvic inflammatory disease [13]. In men, *T. vaginalis* can cause urethral irritation, mild discharge, or burning after urinating or ejaculating, epididymitis, and prostatitis. However, ~85% of women and ~77% of men may be asymptomatic carriers [14,15]. *T. vaginalis* infection is also associated with infertility, preterm birth, low birth weight, and increased susceptibility to human immunodeficiency virus (HIV) infection and transmission [13,15]. It is considered a risk factor for cervical and prostate cancer [13].

In *T. vaginalis*, autophagy has been described as an adaptive mechanism under several nutrient conditions, including low and high glucose, or low and high iron [16–18]. Two autophagy marker proteins have been characterized: TvAtg8a (**TVAGG3_0691340)** and TvAtg8b **(TVAGG3_0430750).** TvAtg8a is associated with autophagosomes under glucose restriction (GR) conditions, while under high glucose (HG) conditions, autophagy is activated as a compensatory proteolytic degradation system when proteasome activity is inhibited [17]. TvAtg8b is another autophagy marker that is induced under GR conditions or iron restriction (IR), and in the presence of rapamycin. TvAtg8b was identified in lysosomes, and lipidated and non-lipidated forms were detected under the different autophagy-inducing conditions tested [18]. Together, these results show that autophagy in *T. vaginalis* can be induced through several signaling pathways [16–18]. Although the processing of the ATG8 family of proteins at the C-terminal end must be carried out by a protease of the C54 family of autophagins, so far, the participation of autophagin-like proteases in the processing of the TvAtg8a and TvAtg8b proteins in *T. vaginalis* has not been reported.

Genomic sequences that encode five TvAtg4-type proteins called TvAtg4.1 (TVAGG3_0280010), TvAtg4.2 (TVAGG3_0421160), TvAtg4.3 (TVAGG3_0930750), TvAtg4.4 (TVAGG3_0673040), and TvAtg4.5 (TVAGG3_0264470) have been found in the genome of *T. vaginalis*. Transcriptomic results under GR and HG conditions showed *tvatg4.1* with the highest expression in GR, followed by *tvatg4.4*

 doi:10.20944/preprints202511.2032.v1

[16]. However, only TvAtg4.4 was detected in the proteomes of parasites grown under different iron conditions [19].

Due to the importance of lipidation of TvAtg8a and TvAtg8b for the autophagic process in this work, we evaluated the processing capacity of the recombinant protease TvAtg4.4 *in vitro* using purified recombinant substrates, rTvAtg8GST and rTvAtg8bGST. In addition, we analyzed the effects of different glucose concentrations on the expression and localization of the TvAtg4.4 protease in *T. vaginalis* under autophagy-inducing conditions. Our results provide insight into the molecular mechanisms of autophagy in *T. vaginalis* by elucidating the enzymatic function and cellular localization of TvAtg4.4, which may have novel roles in parasite biology.

2. Materials and Methods

2.1. In Vitro Cultures of Trichomonas vaginalis

Fresh isolate CNCD 188 of *T. vaginalis* [18] was cultured for one week in tryptone medium with yeast extract (TY) supplemented with 10% heat-inactivated adult bovine serum (HIBS) and 25 mM anhydrous glucose (TYG) (Merck, Darmstadt, Germany) for the normal glucose (NG) condition. For cultures under glucose restriction (GR; ≤1 mM glucose), no glucose was added to the TY medium. For cultures under high glucose (HG) conditions, 50 mM glucose was added. Both cultures were supplemented with 10% HIBS.

2.2. Cloning, Expression, and Purification of Recombinant TvAtg4.4, TvAtg8aGST, TvAtg8bGST, and GST Proteins

Gene sequences of *tvatg4.4* (**TVAGG3_0673040**; 891 bp), *tvatg8a* (**TVAGG3_0691340**; 372 bp), and *tvatg8b* (**TVAGG3_0430750**; 342 bp), added with a GST label at the C-terminal end, were synthesized by Synbio Technologies: Genes for Life company. Codon-optimized genes for *Escherichia coli* were cloned into the transit vector pUC57 with *NcoI* and *XhoI* restriction sites in the 5´ and 3´ ends, respectively. The inserts were recovered and subcloned into the pCri8a [20] expression vector that includes a His_6 tag at its N-terminal end for purification by affinity chromatography (IMAC). The *tvatg8agst-pCri8a*, *tvatg8bgst-pCri8a,* and *tvatg4.4-pCri8a* constructs were transformed into BL21 (DE3) competent bacteria.

The expression of recombinant proteins was induced with 0.1 mM isopropyl-β-D-1-thiogalactopyranoside (IPTG) at 200 rpm for 14 h at 18°C and visualized by SDS-PAGE on 12% polyacrylamide gels stained with Coomassie brilliant blue (CBB). To corroborate the expression of recombinant proteins, Western blot (WB) assays were performed using duplicate gels transferred onto 0.22 µm nitrocellulose (NC) membranes, using an α-His_6-tag mouse monoclonal antibody (1:100 dilution; Santa Cruz Biotechnology, US) and a secondary HRP-coupled goat anti-mouse antibody (1:10,000 dilution). Reactivity was detected by chemiluminescence with a Super Signal™ West Pico Plus Chemiluminescent Substrate (Thermo Scientific), and analysis was performed on a ChemiDoc XRS system (Bio-Rad). Expression of the GST protein was made from a pGEX-5X-1 vector (kindly donated by Dr. José Luis Rosales Encina).

Recombinant protein purification was performed on the soluble fraction (SF) by IMAC with an imidazole gradient, with Ni Sepharose 6 Fast Flow (His Trap™ FF; Cytiva) pre-packaged columns and Sephadex G-25 PD-10 desalting columns (GE Healthcare). Purified rTvAtg4.4, rTvAtg8aGST, rTvAtg8bGST, and GST proteins were stored in storage buffer (150 mM NaCl, 1 mM EDTA, 50 mM Tris-HCl, pH 7.2, 0.02% NaN_3, 30% glycerol) at 4ºC.

2.3. Production of Anti-rTvAtg4.4 Specific Antibodies in Mice and Rabbits

To produce polyclonal antibodies against rTvAtg4.4, 15 6-week-old female BALB/c mice (50 µg protein each, subcutaneously) and 1.5 kg 8-week-old male New Zealand rabbits (200 µg protein, intramuscularly) were inoculated. TiterMax Gold (Sigma-Merck) was used as adjuvant. Sera were

 doi:10.20944/preprints202511.2032.v1

collected before (preimmune serum, PI) and two weeks after inoculation. The resulting antisera (R*α*-rTvAtg4.4 or M*α*-rTvAtg4.4) were used in WB and immunolocalization assays, including indirect immunofluorescence (IFA) and immuno-gold-transmission electron microscopy (TEM). Preimmune sera were used as a negative control.

2.4. Enzymatic Assays of rTvAtg4.4 CP Against rTvAtg8aGST and rTvAtg8bGST Substrates

Purified rTvAtg4.4 was incubated with varying concentrations of purified rTvAtg8aGST or rTvAtg8bGST in buffer A (150 mM NaCl, 1 mM EDTA, 1 mM DTT, 50 mM Tris-HCl, pH 7.2) in a final volume of 21-µL at 37°C for different times. Enzymatic reactions were stopped by adding Laemmli buffer and boiling for 5 min [21], and substrate processing was visualized by SDS-PAGE on 12% polyacrylamide gels stained with CBB. Protein bands were analyzed with Quantity One Software (Bio-Rad). Densitometric analysis was performed using Image Lab 6.1 Security Edition for Windows.

2.5. FarWestern Blotting (FWB) Assay

To determine if the rTvAtg4.4 protein interacts with rTvAtg8aGST and rTvAtg8bGST, a FWB assay was performed. rTvAtg8aGST or rTvAtg8bGST proteins (1 µg per lane) were transferred onto 0.22 µm NC membrane, stained with Ponceau red (PR), blocked overnight (O/N) with 10% skim milk (Gibco) in 0.01% PBS-Tween (PBS-T), washed with PBS-T, and incubated with rTvAtg4.4 (60 µg/mL per lane) or with rChagasin [22] in BSA at 1% in PBS-T at 4°C O/N. Membranes were washed with PBS-T and incubated at 4°C O/N with the primary M*α*-rTvAtg4.4 (1:1000 dilution) antibody. As positive controls, the membranes were incubated directly with R*α*-rTvAtg8a or R*α*-rTvAtg8b (1:5000 dilution) antibodies [18] and with the M*α*-rChagasin (1:1000 dilution) antibody as a negative control [22]. Membranes were washed with PBS-T, incubated with the secondary HRP-coupled goat anti-rabbit or anti-mouse antibody (1:10,000 dilution) for 2 h at 37°C, washed with PBS-T, developed with by chemiluminescence, captured on the ChemiDoc XRS system (Bio-Rad), and analyzed with the Quantity One software (Bio-Rad).

2.6. qRT-PCR Assay

Total RNA was extracted from 2 x 10^7 parasites cultured under GR and HG conditions using TRizol (TRizol Reagent; Ambion, Life Technologies) according to the manufacturer® instructions and treated with DNase. For the cDNA synthesis, the SCRIPT cDNA Synthesis Kit (Jena Bioscience; Building Blocks of Life) was used following the manufacturer® instructions, using 10 µg of total RNA and incubating at 42°C for 10 min, 50°C for 1 h, and 70°C for 10 min to inactivate the enzyme.

For qRT-PCR, the SybrMaster highROX (Jena Bioscience) qPCR kit was used with 100 ng of GR and HG cDNA to amplify a 102 bp *tvatg4.4* fragment using specific primers: sense Fw: 5′-TCTGAGGCATGTGGGCTTTC-3′ and antisense Rv: 5′-GCCCCAACCTGAATCCGAA-3′. Amplification conditions were as follows: 1 cycle at 95 °C for 2 min, followed by 15 s at 95°C and 1 min at 60°C for 40 cycles in an Applied Biosystems®Step One ™ equipment (kindly loaned by Dr. Fidel Hernandez Hernandez). As a normalizing gene, the 101 bp of *α*-tubulin transcript was amplified, using specific primers: sense Fw: 5′-TGCCCAACAGGCTTCAAGAT-3′ and antisense Rv: 5′-TTAGCGAGCATGCAGACACAGC-3′ [23]. The data were analyzed using GraphPad Prism 8.0.1 with the double-delta CT (ΔΔCT) method. Three independent assays were conducted in duplicate.

2.7. Total Protein Extracts for SDS-PAGE Analysis

To obtain total protein extracts (TPE) from parasites grown under GR and HG conditions, 2 x 10^7 parasites were precipitated with 10% trichloroacetic acid (TCA) at 4°C O/N. Samples were centrifuged at 13,000 x g at 4°C for 5 min, the supernatant was removed, and the pellet was washed five times with PBS. The samples were resuspended in 1x Laemmli sample buffer, and protein concentration was quantified using a Nanodrop 2000 spectrophotometer (Thermo Scientific™).

 doi:10.20944/preprints202511.2032.v1

Bromophenol blue and β-mercaptoethanol were added to the proteins, which were boiled for 5 min. 75 μg protein was loaded per lane and separated by SDS-PAGE on a 12% polyacrylamide gel and stained with CBB. Duplicate gels were transferred onto 0.22 μm NC membranes for WB assays.

2.8. Western Blot (WB) Assay

NC membranes containing TPE were incubated with the Mα-rTvAtg4.4 antibody (1:25 dilution) or PI serum or only with the secondary antibody as a negative control, at 4°C for 20 h, washed with TBS-Triton 0.5%, incubated with secondary HRP-coupled goat anti-mouse IgG (H + L) antibody (1:10,000 dilution) (Bio-Rad) at 37°C for 90 min, and developed by chemiluminescence in the Chemidoc XRS system (Bio-Rad). Rα-rTvCatD antibody (1:100 dilution) was used as a control for a positive glucose-regulated protein; Rα-rTvCP2 antibody (1:10,000 dilution) was used as a negative glucose-regulated protein; Rα-TvEno antibody (1:20,000 dilution) was used as a loading control [24]. Membranes with primary antibodies were incubated at 4°C O/N, washed with TBS 1x/Triton X-100 0.1%, incubated with secondary HRP-coupled goat anti-rabbit IgG (H + L) antibody (Bio-Rad) (1:10,000 dilution) at 37°C for 90 min, and developed by chemiluminescence.

2.9. Localization of TvAtg4.4 in Trichomonas by Indirect Immunofluorescence Assays

Parasites cultured under different glucose conditions were washed with PBS, transferred on poly-L-lysine-treated coverslips (1:10; Sigma-Aldrich), fixed with 4% formaldehyde in PBS at room temperature (RT) for 30 min, blocked with 20 mM NH_4Cl_2in PBS and permeabilized with 0.2% Triton X-100 at RT for 10 min. Samples were washed with 0.2% BSA in PBS pH 7.0 (BSA-PBS), incubated with the Mα-rTvAtg4.4 primary antibody (1:50 dilution) in BSA-PBS at 4°C O/N, washed with BSA-PBS and PBS, incubated with goat anti-mouse-Alexa Fluor 594 or Alexa Fluor 647 secondary antibody (Invitrogen) for 1 h at RT in PBS, washed with PBS and incubated with Hoechst 33342 nucleus marker (1:2000 dilution) at RT for 15 min, and washed with PBS. Coverslips were mounted with VectaShield mounting medium (Fluorescence H-1000). For double-labeled IFA, after incubation with Mα-rTvAtg4.4 antibody, coverslips were incubated with other primary antibodies, such as Rα-rTvAtg8a (1:100 dilution), or Rα-rTvAtg8b (1:100 dilution), or with Rα-PFOa [25] (1:50 dilution) at 4°C O/N, washed with PBS, and incubated with goat anti-mouse-Alexa Fluor 594 or Alexa Fluor 647 (Invitrogen) and goat anti-rabbit-FITC secondary antibodies. Nucleus staining and coverslip mounting were performed as described above.

For lysosome colocalization assays, parasites were cultured for 12 h with 5 μM LysoTracker Red DND-99 (Invitrogen) in TY-HIBS medium at 37°C, washed with PBS, fixed with 4% formaldehyde at 37°C for 1 h, washed with HBSS (Gibco), permeabilized with 0.1% Triton X-100, washed with HBSS/BSA, blocked with 0.5 M glycine at RT for 1 h, and washed with HBSS/BSA. The parasites were processed for IFA with the Mα-rTvAtg4.4 antibody, as described above.

2.10. Gold Immunolabeling by Transmission Electron Microscopy

Parasites grown under GR and HG conditions were fixed with 4% paraformaldehyde and 0.5% glutaraldehyde in PBS for 1 h at RT, dehydrated with increasing concentrations of ethanol, embedded in LR White resin (London Resin Co. Ltd., UK), and polymerized at 56 °C O/N. Ultrathin (60-nm) sections were mounted on formvar-covered nickel grids. Thin sections were incubated with 50 mM NH_4Cl at RT for 30 min to quench free aldehyde groups. Subsequently, the sections were blocked with 5% pork serum at RT for 90 min and washed. Double labelling was performed by incubating with Mα-rTvATG4.4 antibody (1:50 dilution) and Rα-rTvATG8a (1:100 dilution), or Rα-rTvATG8b (1:100 dilution), or Rα-PFOa (1:50 dilution) antibody at 4 °C O/N and with a 30-nm gold-conjugated anti-mouse secondary (Ted Pella Inc., CA, USA) and 15-nm gold-conjugated anti-rabbit secondary (1:90 dilution) (Ted Pella Inc., CA, USA) antibodies at RT for 1 h. Samples incubated only with gold-conjugated secondary antibodies were used as negative controls. Sections were contrasted with

 doi:10.20944/preprints202511.2032.v1

uranyl acetate and lead citrate and observed with a JEOL JEM-1011 transmission electron microscope (JEOL Ltd., Tokyo, Japan).

2.11. Statistical Analysis

All results were analyzed using GraphPad Prism Software, versions 8.0.1 and 9.0.1. Statistically significant differences were determined using analysis of variance (ANOVA) and Students *t-test* for WB and qRT-PCR results, respectively.

For the enzymatic assays, nonlinear regression was performed based on the Michaelis-Menten equation. For the enzymatic inhibition assays, a one-way ANOVA was used, followed by Dunnett's multiple-comparison test. Levels of statistical significance are indicated by asterisks in the figure legends.

3. Results

3.1. In Silico Analysis of the Genomic Sequence of T. vaginalis Autophagins

T. vaginalis has five autophagin genes, called *tvatg4.1* (**TVAGG3_0280010**), *tvatg4.2* (**TVAGG3_0421160**), *tvatg4.3* (**TVAGG3_0930750**), *tvatg4.4* (**TVAGG3_0673040**), and *tvatg4.5* (**TVAGG3_0264470**). Each gene encodes a cysteine protease (CP) of the C54 family of autophagins, which is involved in the lipidation and delipidation of TvATG8 proteins, a key process in autophagy [16–18]. Bioinformatic analysis showed that these genes encode for proteins of 285-298 amino acids and include the auxiliary domain (gray) and the protease domain (blue) containing the catalytic triad Cysteine (Cys), Aspartic Acid (Asp), and Histidine (His), characteristic of the C54 family of CPs [26], as shown in Figure 1. Likewise, the evolutionarily conserved motifs cLIR (pink) and APEAR (light blue) were identified. These motifs are key for the recruitment of autophagins to autophagosomal membranes and the direct binding to ATG8/LC3-type proteins [26]. All proteins possess the putative tryptophan (W; yellow) regulator of protease activity, characteristic of autophagins that are self-inhibited by steric impediment (Figure 1C) [26–28]. Comparison of the HsATG4B crystal structure (Figure 1A) [26] with the *in silico* models of all *T. vaginalis* TvAtg4 autophagins from the AlphaFold database showed conservation between the auxiliary and the protease domains (Figure 1B). Regarding the secondary structure, HsATG4B has 8 α-helices and 13 β-sheets (Figure 1D), while TvAtg4 proteins vary in the number of α-helices (11-13) and β-sheets (9-13). Despite this, these proteins showed structural similarity to the crystallized HsATG4B human protein (Figure 1B).

From here on, our analysis focused on the *tvatg4.4* (TVAGG3_0673040) gene and the encoded protein TvAtg4.4. This 891 bp gene lacks introns and is on the antisense strand, spanning 9723524-9724414. At the 5′ and 3′ ends, it is flanked by a sequence encoding a vesicle fusion protein and a GspF protein, respectively (Figure 2Aa). The 5′ intergenic region is 326 bp. The classic transcription initiation Inr promoter element for *T. vaginalis* (TCACT) was identified [29]. Additionally, 8 bp upstream of the translation start codon, the M5 motif (CCTTT) was also found, which is considered as an alternative initiator element specific to the gene family (Figure 2Ab) [29,30]. The 3′ intergenic region is 661 bp. A putative polyadenylation (PS) signal was identified at 35 bp downstream of the stop codon. The putative cleavage site was not identified, but a U-rich region was observed at the expected position [31]. Despite this, the mRNA is polyadenylated, as it was amplified from cDNA generated with an oligo (dT) primer (Figure 2Ab). Therefore, data suggest that there is a non-canonical sequence between the PS and the DSE that could function as a cleavage site (Figure 2Ac).

In silico analysis of the TvAtg4.4 aa sequence suggested putative post-translational modification sites (PTMs), such as phosphorylation, glycosylation, palmitoylation, methylation, and acetylation (Figure 2B), based on a score >0.5. In the predicted TvAtg4.4 3D model, the protease domain has the catalytic triad characteristic of this family (Cys^{52}/His^{216}/Asp^{214}). We also identified the regulatory Trp^{116} close to the catalytic triad. Additionally, conformation of the auxiliary domain is very similar to the crystallized human HsATG4B structure (Figure 2C; Figure 1A; Figure 1Bd) [26,28].

 doi:10.20944/preprints202511.2032.v1

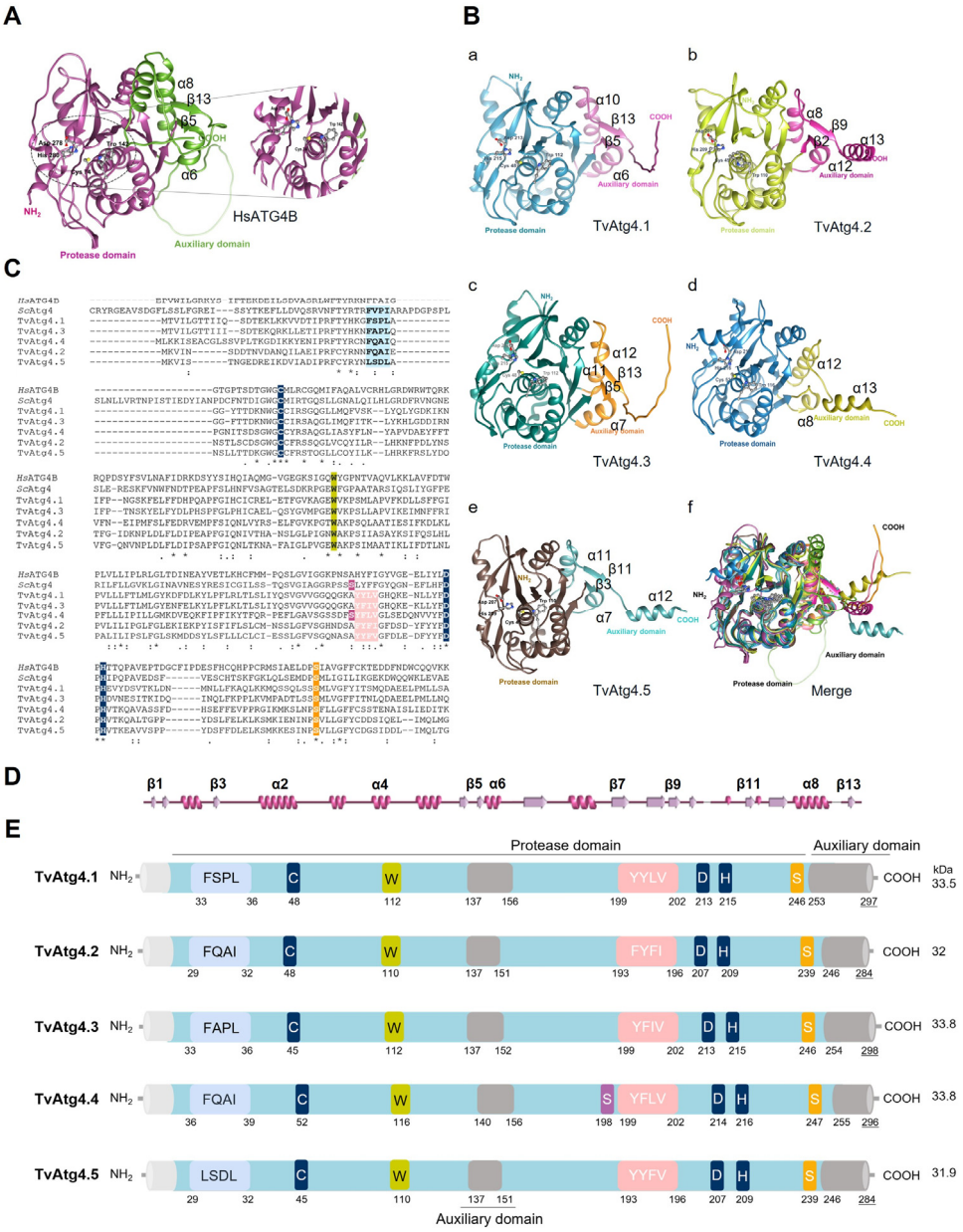

Figure 1. In silico analysis of 3D and 2D structures of TvAtg4 autophagins from *T. vaginalis* and comparison to *Homo sapiens* ATG4B. (A) 3D structure of *Homo sapiens* ATG4B (HsATG4B) obtained from the AlphaFold database (Uniprot Q9Y4P1). The protease domain is presented in magenta and the auxiliary domain in green. The catalytic domain is amplified to show the catalytic triad Cys/His/Asp and the regulatory tryptophan (Trp142). **(B)** 3D modeling of the five TvAtg4 autophagins in PDB format obtained from the AlphaFold database (a) TvAtg4.1 (TVAGG3_0280010), (b) TvAtg4.2 (TVAGG3_0421160), (c) TvAtg4.3 (TVAGG3_0930750), (d) TvAtg4.4 (TVAGG3_0673040), and (e) TvAtg4.5 (TVAGG3_0264470). (f) Overlap of all 3D models of TvAtg4 autophagins (presented in different colors) with HsATG4B using the UCSF Chimera® program. **(C)** Multiple alignment of the amino acid sequences of the five TvAtg4 autophagins with *H. sapiens* HsATG4B, and yeast SCAtg4 (Uniprot Q9Y4P1 or PDB 2CY7). The catalytic triad (Cys, Asp, and His) is highlighted in blue; the regulatory Trp (W142) in yellow; the conserved phospho-serine site of HsATG4B in orange, and that corresponding to yeast in purple. TvAtg4 autophagins share 25% identity with HsATG4B and 23% with yeast Atg4. **(D)** Diagram of *Hs*ATG4B secondary structure. **(E)** Functional domains of TvAtg4 autophagins. The protease domain (blue) and auxiliary domain-like (gray), conformed by two β-strands (β5 and β13) and two α-helices (α6 and α8), except for TvAtg4.4, which does not have the β5 and β13 strands. pLIR-like motifs represented the APEAR domain in light blue and the cLIR-like domain in pink. The size and molecular weight (kDa) of each TvAtg4 was taken from the TrichDB database using the corresponding TVAGG3 number.

 doi:10.20944/preprints202511.2032.v1

Based on these findings, it is proposed that activation of the TvAtg4.4 protease can occur when encountering its substrate (TvAtg8a/b). Thus, this enzyme undergoes a conformational change, and the Trp[116] that masks Cys[52] becomes accessible, allowing the protease to perform its enzymatic function, as previously reported in the literature (Figure 2C, zoom) [27,28].

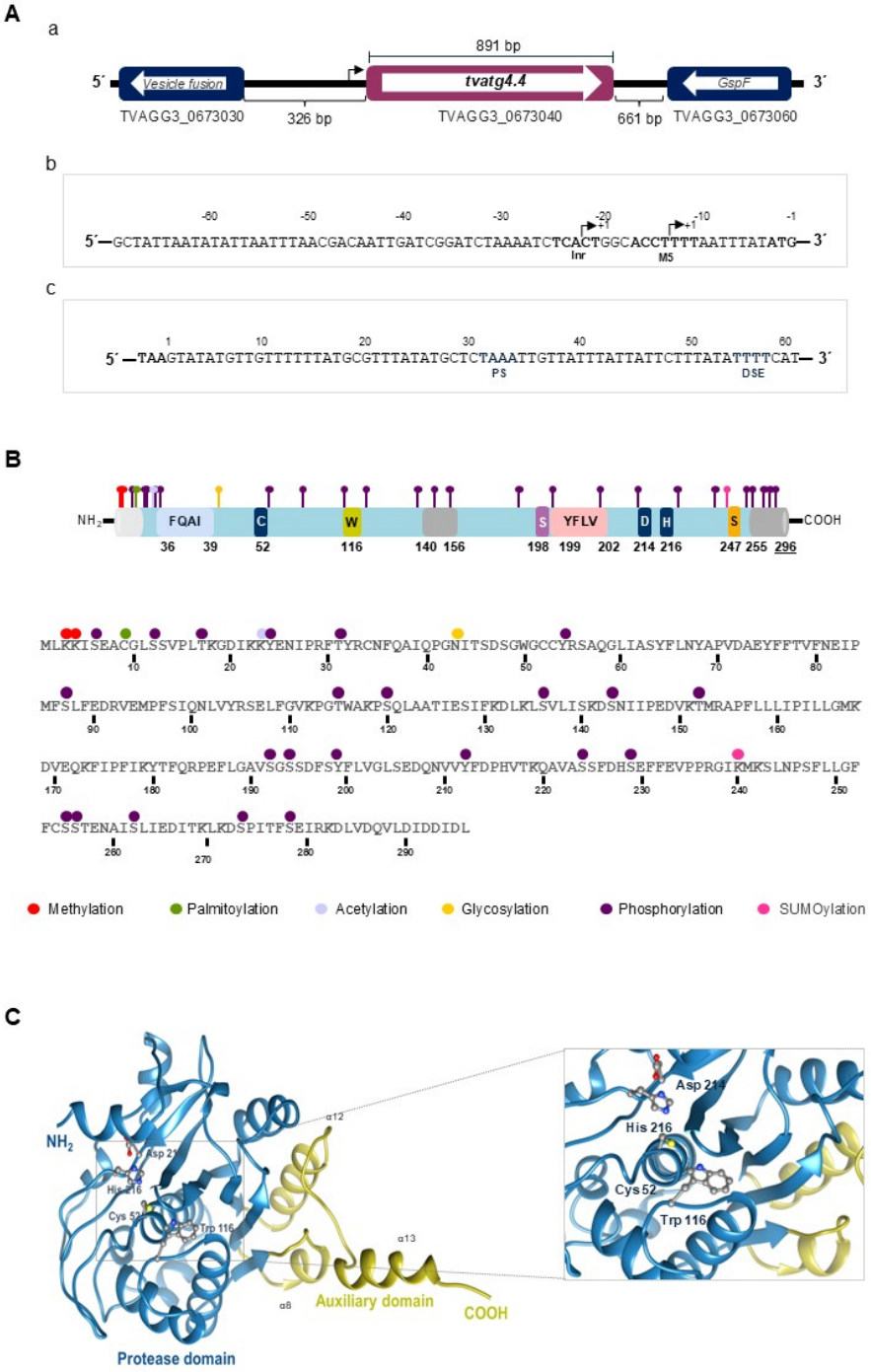

Figure 2. ***In silico*** **analysis of nucleotide and amino acid sequences of TvAtg4.4 from** ***Trichomonas vaginalis*****. (A)** (a) Diagram of the genomic sequence of *tvatg4.4* (TVAGG3_0673040). The gene is 891 bp in size and is flanked in the 5′ end with vesicle fusion protein gene (TVAGG3_0673030) and in the 3′ end with GspF protein gene (TVAGG3_0673060). The intergenic distance is 392 bp and 661 bp, respectively. (b) In the *tvatg4.4* 5′ regulatory region, 11 and 20 bp upstream of the translation start codon (ATG), Inr and M5 motives are highlighted in bold as putative promoter elements for transcription initiation**.** (c) In the *tvatg4.4* 3′ regulatory region, 34 and 54 bp downstream of the stop codon (TAA) is the putative polyadenylation signal, followed by the putative U-rich sequence. **(B)** Diagram of the aa sequence and putative functional domains of the TvAtg4.4 protein showing possible post-translational modifications sites (PTMs): phosphorylation (purple), glycosylation (yellow),

 doi:10.20944/preprints202511.2032.v1

palmitoylation (green), acetylation (lila), SUMOylation (pink), and methylation (red). **(C)** Three-dimensional (3-D) model of the TvAtg4.4 protein in AlphaFold2 v1.5.2. The protease domain is shown in blue and the auxiliary domain in gold. The zoom shows the Cys-Asp-His catalytic triad, as well as the putative regulatory Trp.

3.2. In Vitro Processing of rTvAtg8aGST and rTvAtg8bGST Substrates by rTvAtg4.4 Cysteine Protease

In *H. sapiens*, it has been reported that proteins of the ATG8/LC3 family have a Gly at their C-terminal end, which is recognized by proteases of the C54 family during autophagy. This recognition is necessary for the processing of ATG8 proteins prior to lipidation [32]. *In silico* analysis of the C-terminal end showed that TvAtg8a and TvAtg8b proteins of *T. vaginalis* possess a conserved Gly residue at positions 121 and 111, respectively (Supplementary Figure S1). Therefore, by adding the GST tag at the C-terminal end, the processing of the rTvAtg8aGST and rTvAtg8bGST proteins by rTvAtg4.4 should produce two new bands: i) the GST tag with the two residual aa of the TvAtg8a or TvAtg8b proteins and ii) the remaining aa of rTvAtg8a or rTvAtg8b. Thus, to demonstrate rTvAtg4.4 protease activity, we monitored by SDS-PAGE its processing of the terminal Gly on two constructs with a GST tag added at the C-terminal end of TvAtg8a (**TVAGG3_0691340**) and TvAtg8b (**TVAGG3_0430750**) (Figure 3A). All proteins rTvAtg4.4, rTvAtg8aGST, and rTvAtg8bGST were expressed using a heterologous expression system in *E. coli*, and proteins in soluble fractions were purified by nickel affinity chromatography (Supplementary Figure S2).

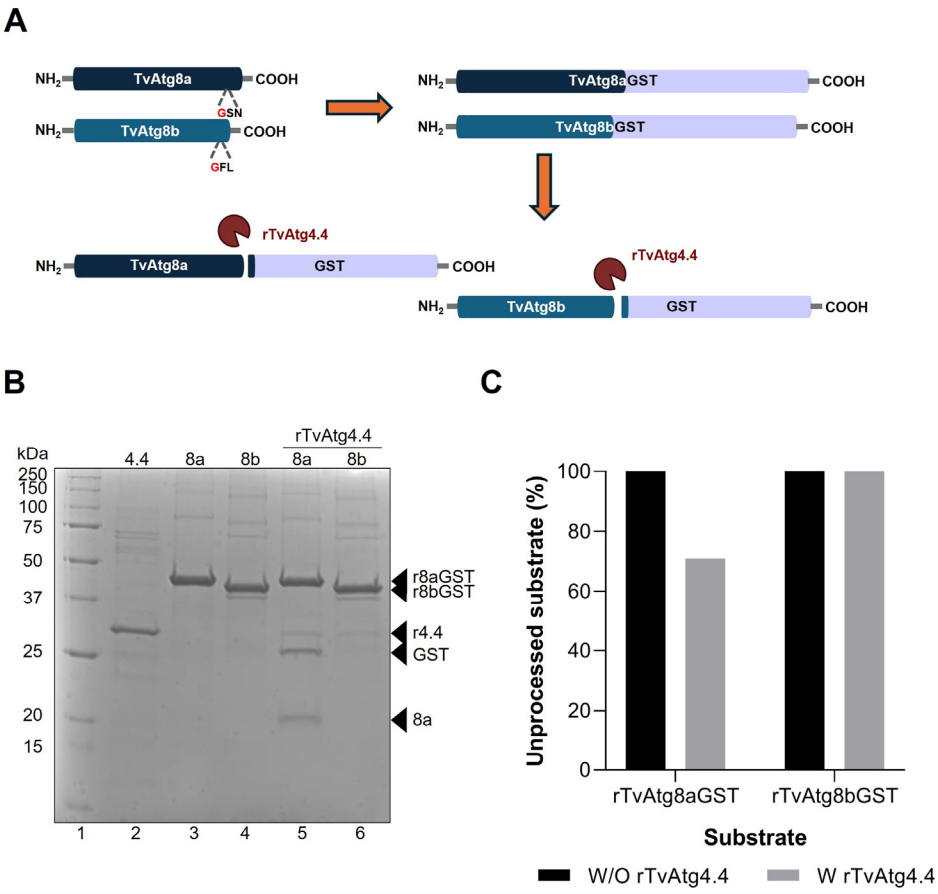

Figure 3. ***In vitro*** **enzymatic processing of rTvAtg8aGST and rTvAtg8bGST proteins by rTvAtg4.4 autophagin. (A)** Diagram of the design of recombinant proteins TvAtg8a and TvAtg8b with the fused GST tag at the carboxyl terminus. The cleavage site of TvAtg4.4 at the G (Gly) residue is shown in red at the carboxyl terminal generating two products: the GST tag and TvAtg8a or TvAtg8b. **(B)** *In vitro* processing of rTvAtg8a/bGST by rTvAtg4.4. rTvAtg4.4 (lane 2) was incubated with either rTvAtg8a/GST and rTvAtg8b/GST (lanes 3 and 4, respectively). The resulting digestion products are shown in lanes 5 and 6. When incubated with rTvAtg8a/GST, rTvAtg4.4 produced the release of GST and TvAtg8a (lane 5, arrowheads). However, no

 doi:10.20944/preprints202511.2032.v1

digestion products were obtained using rTvAtg8bGST as substrate (lane 6). **(C)** Densitometric analysis of rTvAtg8aGST or rTvAtg8bGST protein bands with and without incubation with rTvAtg4.4. The percentage of protein that remained unprocessed was plotted.

To demonstrate the protease activity of rTvAtg4.4 on rTvAtg8aGST (~44 kDa) and rTvAtg8bGST (~43 kDa), rTvAtg4.4 was incubated with each substrate for 1 h at 37ºC and analyzed by SDS-PAGE. Figure 3 shows that rTvAtg4.4 selectively processed rTvAtg8aGST, showing two bands, the GST tag (~26 kDa) and the TvAtg8a (~18 kDa) after incubation with this substrate. However, under the same conditions, no processing of rTvAtg8bGST (43 kDa) by rTvAtg4.4 was detected (Figure 3B). These results were corroborated by densitometric analysis of the rTvAtg8aGST or rTvAtg8bGST unprocessed bands, which showed a 30% reduction for rTvAtg8aGST and no change for rTvAtg8bGST (Figure 3C). Moreover, to corroborate that the released bands corresponded to GST and TvAtg8, WB assays of duplicate gels from the enzymatic assays were performed, using specific antibodies against the proteins rTvAtg4.4, rTvAtg8a, rTvAtg8b, and rGST. Supplementary Figure S3 shows that each band was recognized by the corresponding antibody, as expected.

3.3. The Proteolytic Activity of rTvAtg4.4 is Concentration-Dependent

In the previous assay, it was observed that only rTvAtg8aGST was a specific substrate for rTvAtg4.4, but not for rTvAtg8bGST. To corroborate whether this could be due to an insufficient concentration of protease, enzymatic assays were carried out, varying the concentration of rTvAtg4.4 protease, while maintaining a fixed substrate concentration. Figure 4 shows that when increasing the protease concentration rTvAtg8aGST processing also increased (Figure 4A). However, even at the highest enzyme concentration tested, no processing of rTvAtg8bGST was observed (Figure 4B). The densitometric analysis of the released bands was plotted as the percentage of substrate remaining unprocessed versus the enzyme concentration used, showing that the amount of rTvAtg8aGST decreased with increasing enzyme concentration. However, above 1.6×10^{-8} mM, substrate processing remained constant, with no greater product release (Figure 4C), whereas for rTvAtg8bGST, the percentage of product remained unchanged, with no protease processing detected. In addition, the reaction rates of each enzymatic reaction were plotted using released GST as a reference (Supplementary Figure S4). For rTvAtg8aGST, the reaction rate seems to reach protease saturation at the concentration of 1.6×10^{-8} mM, while the reaction rate of rTvAtg8bGST is maintained at 0 (Figure 4D). Based on these results, under these reaction conditions, only the rTvAtg8aGST protein is a substrate for the rTvAtg4.4 autophagin.

 doi:10.20944/preprints202511.2032.v1

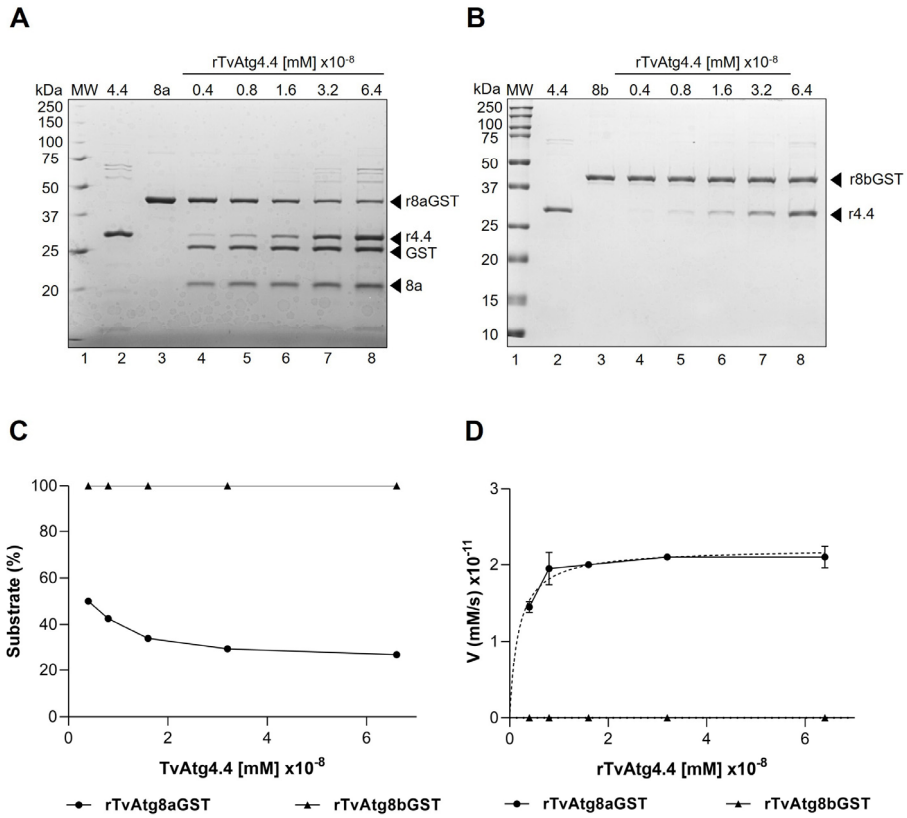

Figure 4. Effect of rTvAtg4.4 concentration on the processing of rTvAtg8aGST and rTvAtg8bGST. Protease activity of rTvAtg4.4 on rTvAtg8aGST **(A)** or rTvAtg8bGST **(B)**. Increasing concentrations of rTvAtg4.4 were added to rTvAtg8a/bGST substrate. Arrowheads indicate the release of the GST tag and TvAtg8a (**A**, lanes 4-8) or unprocessed rTvAtg8b (**B**, lanes 4-8). As a control rTvAtg4.4 was incubated without substrate (lane 2) and rTvAtg8a/bGST without protease (lane 3). **(C)** Densitometric analysis of the released bands was performed. The percentage of unprocessed substrate was calculated using the following formula: ODAtg8s-GST/(ODAtg8s-GST + ODGST + ODAtg8s) × 100%. **(D)** Reaction speed (y-axis) was calculated considering the change in GST concentration and plotted against the different concentrations of rTvAtg4.4 (x-axis). Curves were adjusted using nonlinear regression.

3.4. Effect of Time on rTvAtg4.4 Proteolytic Activity Towards rTvAtg8aGST and rTvAtg8bGST Substrates

Once we identified that the rTvAtg4.4 autophagin can specifically process the rTvAtg8aGST substrate, and that the enzyme concentration determines the processing efficiency, we further evaluated the effect of time on the processing of both rTvAtg8aGST and rTvAtg8bGST substrates. A reaction mix was prepared with 1.6 x 10^{-8} mM rTvAtg4.4 and 4.3 x 10^{-8} mM rTvAtg8aGST or 4.4 x 10^{-8} mM rTvAtg8bGST, incubated at different times (Figures 5A and 5B). Figure 5 shows that for rTvAtg8aGST, the protease had the highest processing efficiency at 30 min. After 45 min, the released products (TvAtg8a and GTS) showed no apparent change, suggesting that rTvAtg4.4 reached saturation (Figure 5A, lanes 4-9). Densitometry analysis of the bands indicated the percentage of substrate that remained unprocessed, and the concentration of GST [mM] released at different times (Figure 5C). Interestingly, incubating rTvAtg8bGST with rTvAtg4.4 for longer times, allowed processing and release of GST and TvAtg8b products (Figure 5B; lanes 4 to 8; Supplementary Figure S3), which was confirmed by densitometry (Figure 5D). The unprocessed substrate stabilized between 12 and 24 h. GST [mM] released curve shows an increase between 0 and 6 h, a decrease between 6 and 12 h, as the enzyme approached its maximum processing capacity, and a plateau from 12 h on, suggesting that the reaction is stabilized by saturation (Figure 5D). These results indicate that the rTvAtg8bGST protein is also a substrate for the rTvAtg4.4 autophagin, but it requires longer incubations.

 doi:10.20944/preprints202511.2032.v1

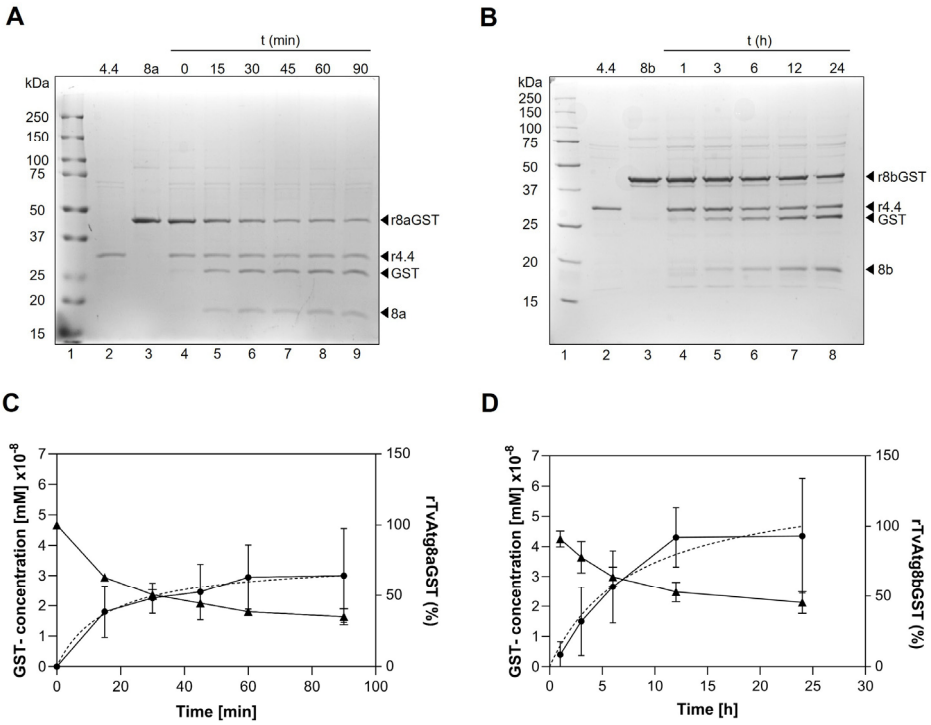

Figure 5. Time-lapse enzymatic activity of rTvAtg4.4 on rTvAtg8aGST (A) or rTvAtg8bGST (B). rTvAtg4.4 (1.66 x 10^{8} mM) was incubated with rTvAtg8aGST (4.37 x 10^{8} mM) or rTvAtg8bGST (4.425 x 10^{-8} mM) at 37°C for 0, 15, 30, 45, 60, and 80 min for rTvAtg8aGST (A, lanes 4 to 9); and 1, 3, 6, 12, and 24 h for rTvAtg8bGST (B, lanes 4 to 8). Reactions were stopped by boiling for 5 min and the release of GST tag and TvAtg8a or TvAtg8b protein was visualized on 12% SDS-PAGE. **(C and D)** The percentage of rTvAtg8aGST (**C**) or rTvAtg8bGST (**D**) that remains unprocessed was calculated by the amount of released GST in mM concentration versus the incubation time using the following equation: ODAtg8s-GST/(ODAtg8s-GST + ODGST + ODAtg8s) × 100%. Data were plotted with a nonlinear regression.

3.5. Enzymatic Kinetics for rTvAtg4.4 Autophagin

We determined the rate at which the rTvAtg4.4 autophagin catalyzes the processing of rTvAtg8aGST (Vmax) and the enzyme's affinity, as measured by the Michaelis-Menten constant (Km). To do this, we incubated different concentrations of rTvAtg8aGST with rTvAtg4.4 protease [1.6 x 10^{-8} mM] for 30 min. Figure 6A shows that at low rTvAtg8aGST concentrations, the rate of the reaction (substrate processing) rapidly increased (Figure 6A, lanes 4 to 7). However, at higher substrate concentrations, the enzyme appears to become saturated, suggesting that the protease is close to its maximum processing capacity (Figure 6A, lanes 8 and 9). A quantitative analysis was performed by densitometry of the bands (Figure 6B). First, to analyze unprocessed versus processed substrates, a nonlinear regression was performed, considering the amount of GST released, to obtain the Vmax (9.6 x 10^{-11} mM/s) and the Km (9.9 x 10^{-8} mM) values (Figure 6B). The rTvAtg4.4 autophagin Km value suggests that this autophagin has a high affinity for the rTvAtg8aGST substrate, since a low concentration of the protease is needed to reach half of its maximum activity. Moreover, the rTvAtg4.4 Vmax value indicates that it can achieve its activity within the estimated range. These data confirm that the TvAtg4.4 autophagin has *in vitro* protease activity towards both substrates (rTvAtg8aGST and TvAtg8bGST), with rTvAtg8aGST as the preferred substrate in <1 h.

 doi:10.20944/preprints202511.2032.v1

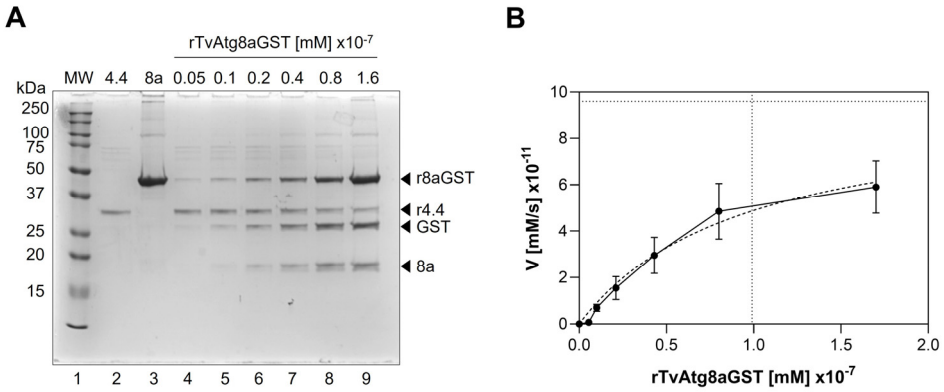

Figure 6. Enzymatic kinetics of the rTvAtg4.4 autophagin to determine its Km and Vmax values. (A) TvAtg4.4 autophagin (1.66 x 10^{-9} mM) was incubated with 0.05, 0.1, 0.2, 0.4, 0.8, and 1.6 x 10^{-7} mM; rTvAtg8aGST, and the digestion products were analyzed by SDS-PAGE (lanes 4-9). As reaction controls, we used the maximum concentration of substrate without enzyme (lane 3) and enzyme without substrate (lane 2). **(B)** The percentage of substrate that remains unprocessed was calculated by plotting the different concentrations against the total amount of substrate in the reaction. The maximum rate of reaction was defined as the change in the concentration of released GST, and the values obtained were plotted against the different substrate concentrations used. The curves were fitted using the nonlinear regression method for enzyme kinetics to determine the Michaelis-Menten data.

3.6. Interaction of rTvAtg4.4 Autophagin with rTvAtg8aGST and rTvAtg8bGST Substrates

To demonstrate that rTvAtg4.4 autophagin is a CP, the protein was treated with the following protease inhibitors: Metallo- (EDTA), serine- (TLCK), aspartic- (SO_4Cu_2), and CP-type inhibitors (IAM and E-64) for 20 min before adding the rTvAtg8aGST substrate. Enzymatic reactions were visualized by SDS-PAGE (Figure 7A), and the raw substrate band was quantified by densitometry (Figure 7B). The results show that rTvAtg4.4 activity was almost completely inhibited by IAM and partially by E-64 (Figure 7A, lanes 8 and 9), as the intensity of the bands of the released products (TvAtg8a and GST) decreased, while other inhibitors did not affect the released products bands and a reduced substrate band was observed (Figure 7A; lanes 5-7). Densitometric analysis showed the unprocessed substrate remaining after the enzymatic reaction, using the inhibitors (Figure 7B). Taking together, these results confirm that rTvAtg4.4 is a CP-like protease.

To demonstrate the substrate specificity of the rTvAtg4.4 autophagin, a reaction mixture with albumin (BSA) was performed and compared with the rTvAtg8aGST specific substrate (Figure 7C, lanes 3 and 4). The results showed that rTvAtg4.4 protease processed only rTvAtg8aGST, yielding the expected GST and TvAtg8a band products (lane 5), whereas with BSA, no lower molecular weight bands were observed (lane 6). These results demonstrate the substrate specificity of the rTvAtg4.4 autophagin. Figure 7D shows the densitometric analysis of the substrate bands before (lanes 3 and 4) and after the rTvAtg4.4 enzymatic reaction (lanes 5 and 6).

To corroborate the specificity of protein-protein interactions between rTvAtg4.4 autophagin and rTvAtg8aGST or rTvAtg8bGST FarWB assays were performed (Figures 7E and 7F). Interaction of rTvAtg4.4 with both substrates was observed, as revealed by the anti-rTvAtg4.4 antibody detection of rTvAtg8aGST or rTvAtg8bGST only after rTvAtg4.4 interaction (lanes 8), but not when the substrates were not previously exposed to the rTvAtg4.4 protein (lanes 5). Preincubation with the unrelated recombinant protein chagasin did not elicit recognition with the anti-chagasin antibody (lanes 7). As expected, anti-substrate antibodies used as a positive control detected each of them (lanes 6). This result confirms that there is a specific interaction between the proteins rTvAtg8aGST–rTvAtg4.4 and rTvAtg8bGST-rTvAtg4.4.

 doi:10.20944/preprints202511.2032.v1

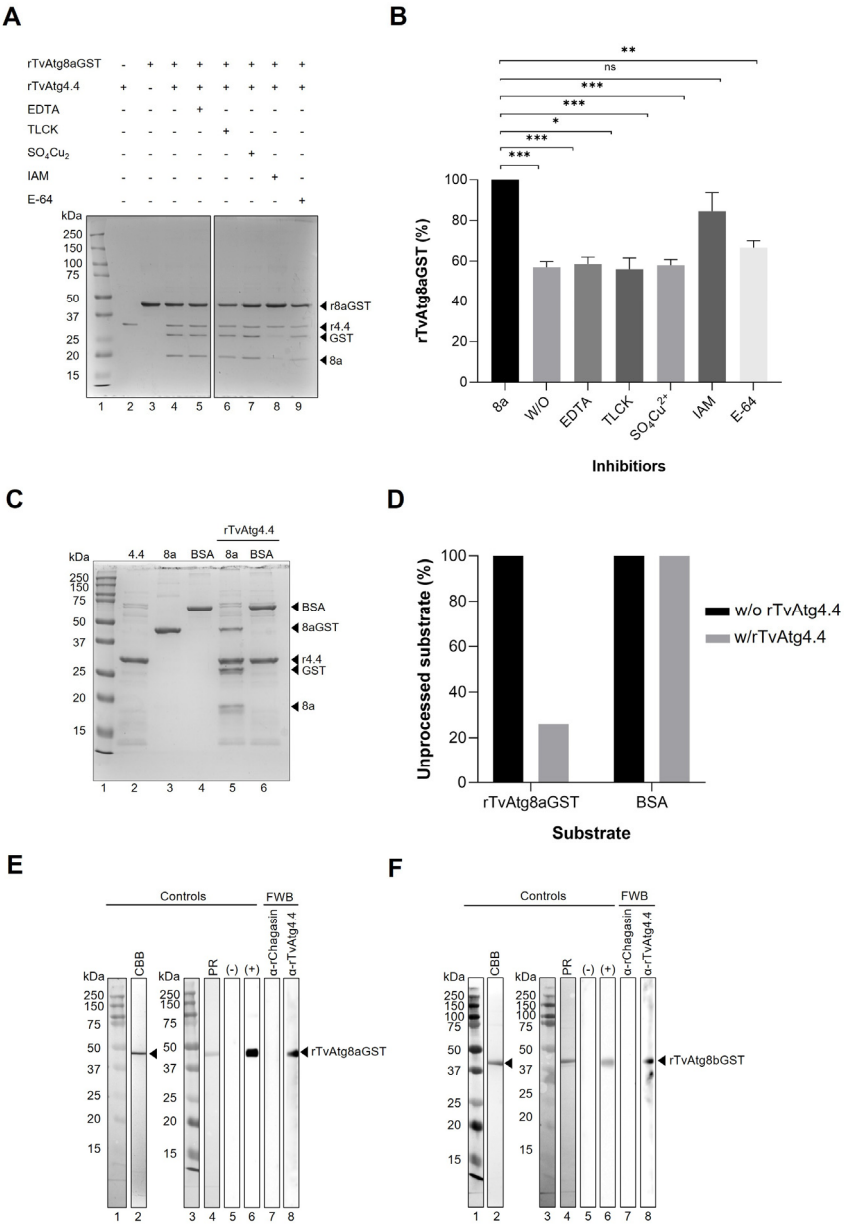

Figure 7. Substrate specificity for rTvAtg4.4 autophagin. (A) Inhibition of the protease activity of the rTvAtg4.4 autophagin using different families of protease inhibitors: metallo (EDTA), serine (TLCK), aspartic (SO_4Cu_2), and cysteine (IAM and E-64). The protease activity was measured by analyzing the amount of rTvAtg8aGST that remained unprocessed. **(B)** The results obtained were plotted as the percentage of rTvAtg8aGST that remained unprocessed in the presence of the different protease inhibitors used. Asterisks denote statistical significance: *** $p<0.001$, ** $p<0.001$, $p<0.01$). **(C)** rTvAtg4.4 autophagin incubated with rTvAtg8aGST protein (lane 5) or BSA (lane 6) in a reaction mix for 1 h at 37°C. The reactions were stopped by boiling for 5 min and separated by 12% SDS-PAGE. As controls, a reaction mix was incubated with only rTvAtg4.4 (lane 2), TvAtg8aGST (lane 3), or BSA (lane 4). **(D)** A densitometric analysis of the unprocessed bands was performed, and the percentage of unprocessed substrate with and without enzyme was plotted. **(E and F)** FarWestern blot (FWB) to detect protein-protein interaction between rTvAtg4.4 autophagin and rTvAtg8aGST (E) or rTvAtg8bGST (F). Substrates were separated by SDS-PAGE, gel strip stained with Coomassie brilliant blue (CBB, lanes 2) and transferred onto nitrocellulose membranes and stained with Ponceu red (PR, lanes 4). As positive controls, the membranes were incubated with anti-rTvAtg8a or anti-rTvAtg8b antibody (lanes 6). For negative controls, the membranes were incubated with the anti–rTvAtg4.4 antibody (lanes 5). For the FWB assay, each substrate membrane was pre-incubated with rTvAtg4.4 (lanes 8) or rChagasin (lanes 7), washed, incubated with anti-rTvAtg4.4 (lanes 8) or anti-rChagasin (lanes 7) antibodies, washed, incubated with HRP–conjugated secondary antibody, and developed by chemiluminescence.

 doi:10.20944/preprints202511.2032.v1

3.7. Effect of Glucose on Tvatg4.4 Transcription

Glucose is the primary carbon source for *T. vaginalis* under both anaerobic and aerobic conditions. To determine the effect of glucose on *tvatg4.4* expression, qRT-PCR was performed using cDNA from parasites cultured under GR and HG conditions. Figure 8A shows a ≥1-fold increase in transcripts from parasites cultured under GR compared to those in HG conditions. The observed differences were significant ($p < 0.0001$) across three independent experiments performed in duplicate. Expression levels of *tvatg4.4* were normalized against *α-tubulin* for each glucose condition. Our results suggest an upregulation in the expression of the *tvatg4.4* gene when *T. vaginalis* is under glucose restriction culture conditions.

3.8. Effect of Glucose on the Amount of TvAtg4.4 Protein

To determine the effect of glucose on the amount of TvAtg4.4 protein, a WB assay was performed using extracts of parasites grown under GR and HG conditions. The specific anti-rTvAtg4.4 antibody detected five protein bands of ~110, ~45, ~35, ~27, and ~22 kDa (Figure 8B). The expected size of native TvAtg4.4 protein in *T. vaginalis* is ~35 kDa (Figure 8B, lanes 14 and 15). The ~110 kDa band could correspond to TvAtg4.4 oligomeric protein, as the formation of high-molecular-weight oligomers via intermolecular disulfide bridges has been reported for other ATG4s, such as HsATG4B [15]. This could be supported by the presence of higher molecular weight bands unable to enter the gel, which were detected by the anti-TvAtg4.4 antibody. This TvAtg4.4 signal was more intense in HG than GR parasite extracts (Figure 8B, lanes 14 and 15 marked with a star). PTMs, such as glycosylation or SUMOylation, could increase the size of the protein and explain the ~45 kDa band. However, the formation of a complex between TvAtg4.4 and either TvAtg8a or TvAtg8b cannot be ruled out, as a mechanism for regulating its enzymatic activity. The ~27- and ~22-kDa bands may correspond to processing products of the TvAtg4.4 protein (Figure 8B, lanes 14 and 15). Bands detected under both glucose conditions were normalized to enolase (TvEno; Figure 8B, lanes 8 and 9). Densitometry analysis showed that no significant differences of the bands obtained from parasites extracts grown under both glucose conditions (Figure 8C). TvCP2 and TvCatD proteins were used as controls for GR and HG conditions, respectively (Figure 8B, lanes 10-13, respectively). Negative controls included incubation with the PI serum or only with the secondary antibody (Figure 8B, lanes 6 and 7). These results were confirmed in three independent experiments.

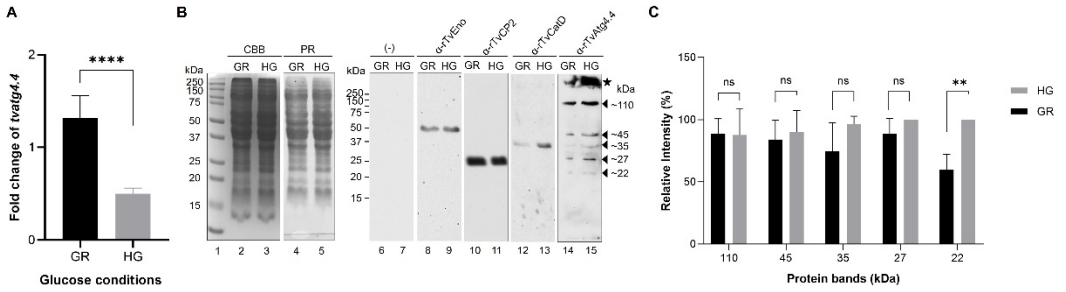

Figure 8. Effect of glucose on transcription and translation of TvAtg4.4 autophagin. (A) using cDNA from parasites grown under glucose-restricted (GR) and high glucose (HG) conditions were used as templates to determine transcription of *tvatg4.4* by qRT-PCR assay using α-tubulin as a normalized gene. Statistical significance is shown with asterisks **** $p<0.0001$. **(B)** WB assay of total protein extracts (TPE) of parasites grown under GR and HG conditions. Lanes 2 and 3, total protein patterns of parasites grown under GR and HG conditions separated by 12% SDS-PAGE stained with CBB. Duplicate gels were transferred onto NC membranes and stained with, Ponceau red (PR, lanes 4 and 5), or incubated only with the secondary antibody (negative control, lanes 6 and 7), and incubated with distinct primary antibodies:, Rα-rTvEno Ab (loading control, lanes 8 and 9); Rα-rTvCP2 Ab (control protein negatively regulated by glucose, lanes 10 and 11); Mα-rTvCatD Ab (control protein positively regulated by glucose, lanes 12 and 13); Mα-rTvAtg4.4 Ab (to detect the TvAtg4.4 protein in trichomonad extracts, lanes 14 and 15). Arrowheads indicate bands identified by the anti-rTvAtg4.4 antibody (~110, ~45, ~35, ~27 y ~22 kDa) in extracts from parasites grown under

 doi:10.20944/preprints202511.2032.v1

GR and HG conditions. Star indicates putative high molecular weight TvAtg4.4 oligomers. **(C)** Densitometric analysis normalized to the enolase band was carried out with each protein band. The band with the highest intensity (pixels) was taken as 100%, for comparative purposes. A statistical analysis was performed, and significant differences are shown with asterisks ** $p < 0.001$.

3.9. Localization of the TvAtg4.4 Autophagin of T. vaginalis Grown Under Different Glucose Conditions

To determine the subcellular localization of TvAtg4.4 in parasites cultured in GR and HG conditions, IFAs were performed in permeabilized parasites and immuno-gold-TEM labeling using the Mα-rTvAtg4.4 antibody (Figure 9). A greater number of vesicles containing TvAtg4.4 per parasite was observed in HG (Figure 9A, m-r) comparable to GR (Figure 9A, g-l) conditions, which could correspond to autophagic vesicles (AV) (Figure 9A, g-r). TvAtg4.4 was also observed in the Golgi apparatus (G) of some parasites grown under HG conditions (Figure 9A Zoom, r, arrowhead). Ultrastructural localization was performed by immuno-gold-TEM labeling (Figure 9B). Under both glucose conditions, TvAtg4.4 was identified in hydrogenosomes (H), cytoplasm (C), vesicles (V), endoplasmic reticulum (ER), Golgi apparatus (G), and close to the membrane (M) (Figure 9B, d-h). The localization of TvAtg4.4 in V and ER in IFA and TEM assays supports our previous reports of an autophagic flux in *T. vaginalis* [18] and is consistent with the process described in *H. sapiens*. In the autophagy mechanism, Abreu et al reported the localization of HsATG4B in the ER and in AV; in the ER, ATG8 is proposed to be cleaved immediately after its synthesis, while the cleavage of ATG8 from the AV outer membrane is necessary for the lysosome to fuse with the autophagosome to form the autophagolysosome [33]. The localization of TvAtg4.4 in *T. vaginalis* hydrogenosomes by TEM is an interesting observation, because it poses the question aands to whether there is another type of autophagy mechanism in *T. vaginalis*, besides the degradative, such as a secretory autophagy taking place in hydrogenosomes [25]. This question needs to be addressed in future experiments.

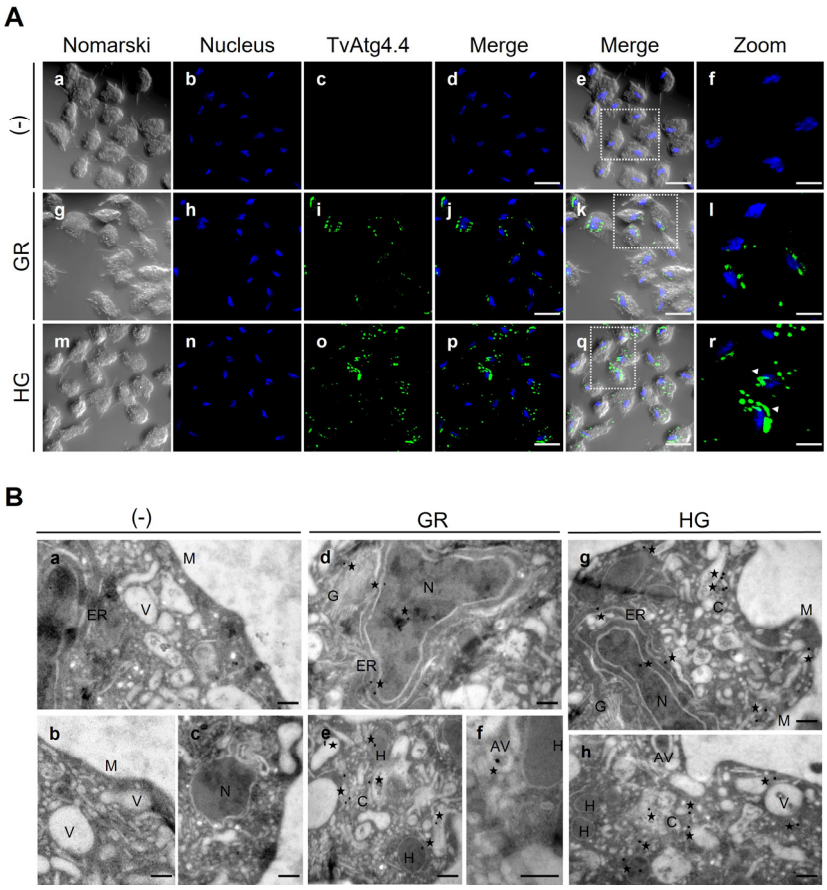

Figure 9. Localization of TvAtg4.4 in *T. vaginalis* grown under GR and HG conditions by IFA and TEM. (A) Permeabilized parasites grown under GR (panels g-l) or HG (panels m-r) conditions were incubated with Mα-

 doi:10.20944/preprints202511.2032.v1

rTvAtg4.4 antibody and a secondary antibody coupled to Alexa-594 (green). As a negative control (-), parasites were incubated only with the secondary antibody (panels c). Nuclei were stained with Hoechst. Orthogonal projection (OP) or optical section (S). Scale bar, 5 μm, except for amplified images (Zoom) that correspond to 2 μm. **(B)** Immuno-gold localization by TEM of parasites grown under GR (panels d–f) and HG (g-h) conditions using the Mα-rTvAtg4.4 antibody and a secondary antibody coupled to 20 nm gold particles. Negative controls (-) were incubated with PI serum or only with the secondary antibody (panels a-c). Cytoplasm (C), nucleus (N), membrane (M), hydrogenosome (H), endoplasmic reticulum (ER), Golgi apparatus (G), vesicle (V), autophagic vesicle (AV). Scale bar, 200 nm.

3.10. TvAtg4.4 Is Localized in Autophagic Vesicles Under Different Glucose Conditions

To analyze whether TvAtg4.4 is indeed an autophagin in *T. vaginalis* through the processing of the autophagy marker proteins TvAtg8a and TvAtg8b, colocalization assays were performed by IFA and immuno-gold-TEM on parasites cultured under GR and HG conditions (Figure 10). By IFA, TvAtg4.4 colocalized with TvAtg8a in vesicles in both GR (Figure 10 h-n; V yellow) and HG (Figure 10 o-u; V yellow) culture conditions, confirming the presence of TvAtg4.4 in AV. In addition, some parasites showed also vesicles with individual labels, TvAtg4.4 (green V) or TvAtg8a (red V), under both glucose conditions.

Colocalization assays of TvAtg4.4 and TvAtg8b revealed the highest colocalization in HG (Figure 10, ac-ai; V yellow) compared to GR (Figure 10, v-ab) conditions. In addition, under HG conditions some vesicles contained only TvAtg4.4 (green V) or, to a lesser extent, TvAtg8b (red V). Vesicles containing only TvAtg4.4 (green V) were observed outside the parasite, suggesting that TvAtg4.4 is actively secreted. Further analysis of these TvAtg4.4-containing released vesicles need to be performed. To quantify the linear relationship between TvAtg4.4 and its substrates, Pearson's coefficient of correlation was calculated. While all results indicated a positive linear correlation (as one variable increases, the other increases), under HG conditions Pearson's coefficient was higher (0.644 for TvAtg8a and 0.748 for TvAtg8b) than under GR conditions (0.484 for TvAtg8a and 0.401 for TvAtg8b (Figure 10).

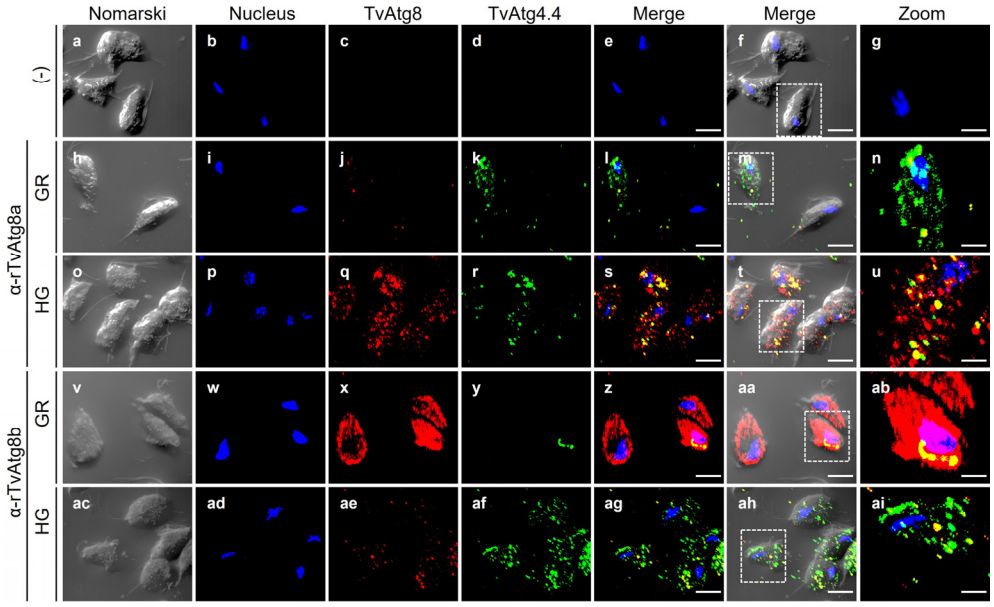

Figure 10. Colocalization of TvAtg4.4 with TvAtg8a or TvAtg8b autophagosomes under GR and HG conditions by IFA. Permeabilized parasites were double labeled with Mα-rTvAtg4.4 antibody (green) and Rα-rTvAtg8a or Rα-rTvAtg8b antibodies (red) to identify autophagic vesicles in parasites grown under GR (h-n and v-ab, respectively) or HG (o-u and ac-ai, respectively) conditions. Colocalization was measured by the Pearson coefficient; a value >0.5 suggests colocalization between proteins. Samples incubated with PI serum or only with the secondary antibody (a-g) were used as negative controls. Scale bar, 5 μm. Zoom bar, 2 μm.

 doi:10.20944/preprints202511.2032.v1

Colocalization of TvAtg4.4 and its substrates TvAtg8a and TvAtg8b was confirmed by immuno-gold-TEM (Figure 11). Under GR and HG conditions, TvAtg4.4 and TvAtg8a or TvAtg8b were found close to the ER, in V, and in the cytoplasm (TvAtg8a, Figure 11, d-i), and in AV, H, and V (TvAtg8b, Figure 11, j-o). These results show that TvAtg4.4 is close to both substrates in ER and AV, where it would be expected during autophagy. However, TvAtg4.4 is also present in other types of vesicles.

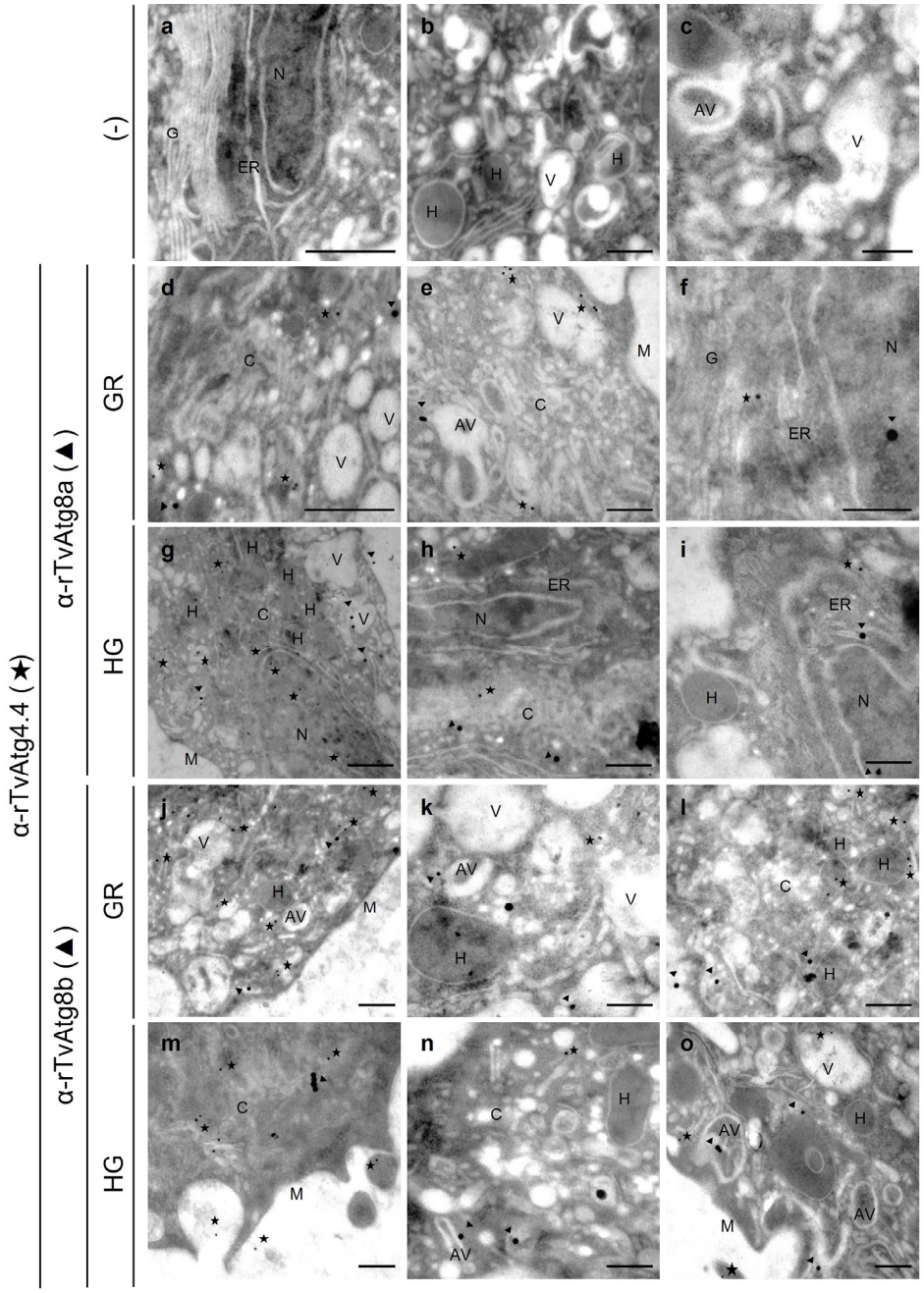

Figure 11. Subcellular localization of TvAtg4.4 with TvAtg8a or TvAtg8b by TEM. Parasites grown under GR and HG conditions were labeled with Mα-rTvAtg4.4 primary antibody and a secondary antibody coupled to 15 nm gold particles (stars), and with Rα-rTvAtg8a or Rα-rTvAtg8b antibodies and a secondary antibody coupled to 30 nm gold particles (arrowheads). (-) PI serum or incubation with only secondary antibody (a-c) was used as a negative control. The organelles were identified as follows: cytoplasm (C), nucleus (N), membrane (M), hydrogenosome (H), endoplasmic reticulum (ER), Golgi apparatus (G), Vesicle (V), autophagic vesicle (AV) in TvAtg8a or TvAtg8b under GR (d-f and j-l) and HG (g-i and m-o) conditions, respectively. Black scale bars, 500 nm and 200 nm.

 doi:10.20944/preprints202511.2032.v1

3.11. Localization of TvAtg4.4 Autophagin in Lysosomes

To determine whether TvAtg4.4 is also localized in trichomonad lysosomes, IFA was performed, using double labelling with lysotracker and anti-rTvAtg4.4 antibody (Figure 12). TvAtg4.4 colocalized with some lysosomes under GR conditions (Figure 12 o-ab). Under HG conditions, the parasites exhibited a greater number of vesicles colocalizing with TvAtg4.4 (Figure 12 ac-ap) than under GR conditions. These results caught our attention because no previous studies had demonstrated that autophagins could be found in lysosomes. So far, *in silico* analysis predicted its possible cytoplasmic location (Uniprot: https://www.uniprot.org/uniprotkb/A2DXA2/entry#subcellular_location). To explain this finding, its degradation by the endolysosomal system could be speculated. However, this could also suggest the existence of a non-canonical secretion route of TvAtg4.4. This is supported by the identification of free TvAtg4.4-containing vesicles outside the parasites in GR and HG conditions (Figure 12 o-ab and ac-ap, respectively), which did not colocalize with the lysosome marker (Figure 12 u and ai, green vesicles, arrowhead).

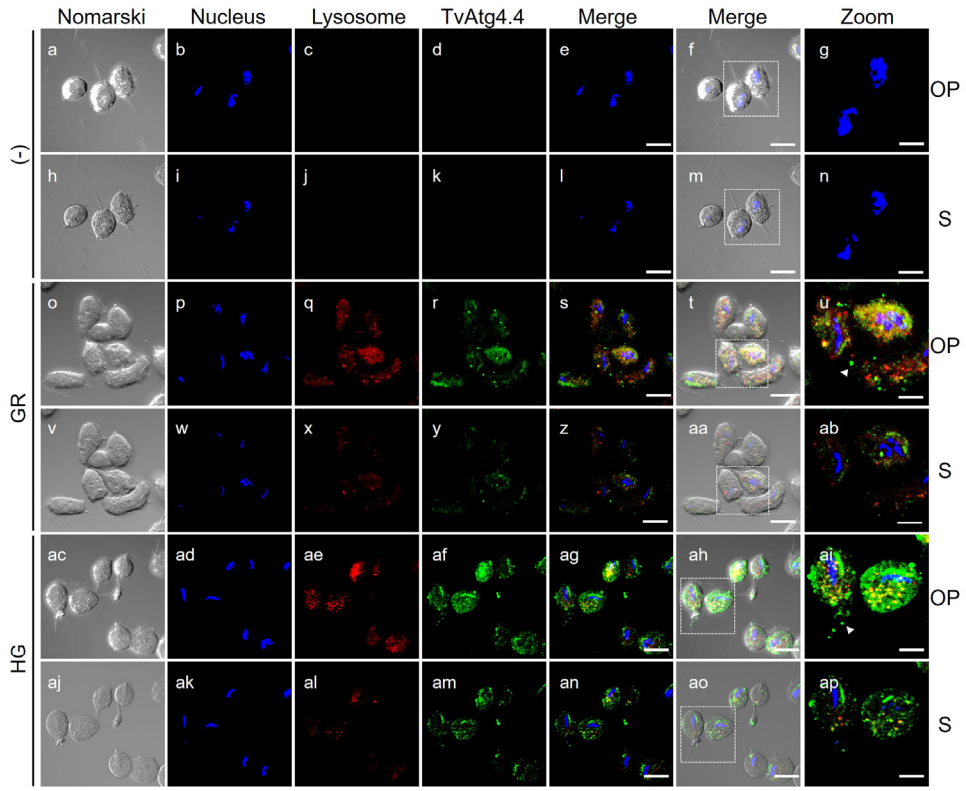

Figure 12. Permeabilized parasites grown under GR (o-ab) and HG (ac-ap) glucose conditions. Parasites were labeled with Mα-rTvAtg4.4 antibody (green) and with Lysotracker (red). (-) Samples incubated with PI serum or only secondary antibody (a-n) were used as negative controls. Nuclei were labeled with Hoechst (blue). Orthogonal projection (OP) and optical sections (S) are shown. Scale bar, 5 μm. Zoom bar, 2 μm.

3.12. Localization of TvAtg4.4 Autophagin in Hydrogenosomes

Moreover, TvAtg4.4 was also identified in hydrogenosomes by IFA and immuno-gold-TEM, using PFOa as hydrogenosome marker [25]. Figure 13 shows greater colocalization of TvAtg4.4 and PFOa in multiple vesicles in GR (Figure 13A, o-ab; V yellow) (Pearson's coefficient of 0.641) compared to HG conditions (Figure 13A, ac-ap) (Pearson's coefficient of 0.287). In a section, the vesicles appear close to the membrane (Figure 13A, ab). Localization of TvAtg4.4 in hydrogenosomes was confirmed by immuno-gold-TEM (Figure 13B) under both glucose conditions. It was observed in roughly 40% of parasites. This observation undoubtedly merits further investigation.

 doi:10.20944/preprints202511.2032.v1

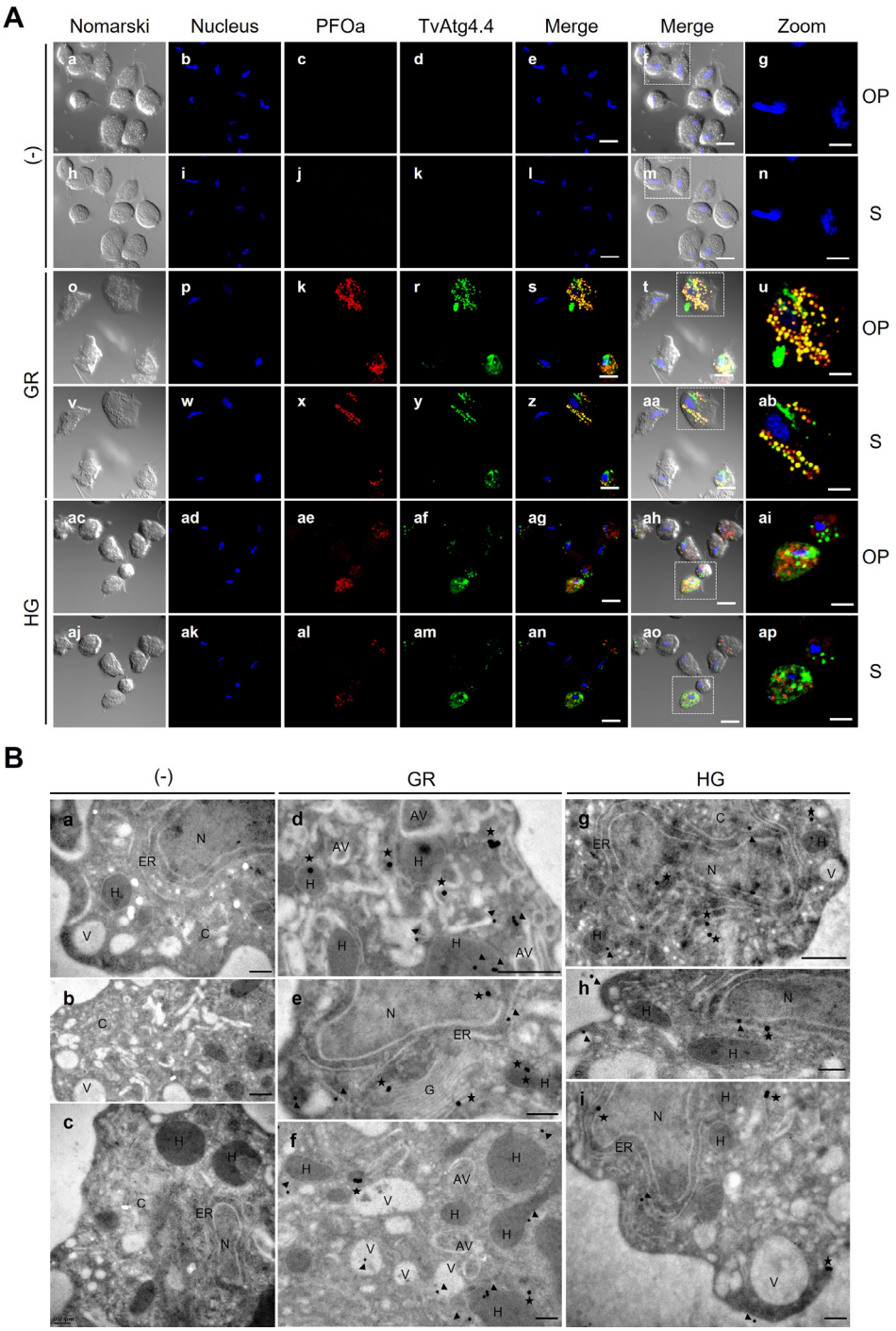

Figure 13. Localization of TvAtg4.4 autophagin in hydrogenosomes of parasites grown under different glucose conditions by IFA and TEM. (A) Permeabilized parasites grown under GR (o-ab) and HG (ac-ap) conditions were labeled with M*α*-rTvAtg4.4 (green) and with R*α*-rPFOa (red) antibodies to identify hydrogenosomes. (-) Incubation with PI serum or only with secondary antibody was used as a negative control (a-n). Nuclei were labeled with Hoechst (blue). Yellow vesicles indicate the localization of TvAtg4.4 in hydrogenosomes. Orthogonal projections (OP) and optical sections (S) are shown. Scale bar 5 μm; Zoom bar 2 μm. **(B)** TEM of parasites grown under GR (d-f) or HG conditions (g-i); (-) parasites incubated only labeled with the secondary antibody (a-c) were used as negative controls. The location of TvAtg4.4 (stars) and PFOa (arrowheads) is indicated. Identified organelles: cytoplasm (C), nucleus (N), membrane (M), hydrogenosome (H), endoplasmic reticulum (ER), Golgi apparatus (G), Vesicle (V), autophagic vesicle (AV). Black scale bar, 500 nm and 200 nm.

 doi:10.20944/preprints202511.2032.v1

4. Discussion

Autophagy is a fundamental process to maintain cellular homeostasis. Different forms of autophagy have been described, and the various pathways followed by each of them have been reported in many eukaryotes. However, the process in lower eukaryotes, such as in the protozoan parasite *T. vaginalis* has only started to be revealed by studying the mechanism of macroautophagy induced by cultivation under low (GR) and high (HG) glucose, or low (LI) and high (HI) iron conditions [16].

During autophagy, membrane elongation, cargo protein recognition, autophagosome closure, autophagosome trafficking, autophagosome-lysosome fusion, and inner membrane degradation involves the ATG8 conjugation system, one of the two ubiquitin-like conjugation systems widely conserved in eukaryotes that are essential during autophagy [9]. Lipidation of ATG8 is necessary to perform its functions, for which an ATG4 protease of the C54 family of autophagins must cleave the C-terminal end of ATG8 to expose a glycine residue (Gly) that allows the addition of phosphatidylethanolamine (PE), a crucial step for the binding of phagophore membranes to form autophagosomes.

Due to the importance of lipidation of TvAtg8a and TvAtg8b for the autophagic process, in this work we evaluated the processing capacity of the recombinant protease TvAtg4.4 *in vitro* using purified substrates, rTvAtg8GST and rTvAtg8bGST. In addition, we analyzed the effects of different glucose concentrations on the expression and localization of the TvAtg4.4 protease in *T. vaginalis* under autophagy-inducing conditions. Our results provide insight into the molecular mechanisms of autophagy in *T. vaginalis* by elucidating the enzymatic function and cellular localization of TvAtg4.4, which may have novel roles in parasite biology.

Five TvAtg4-like proteins have been reported in the genome of *T. vaginalis* (TvAtg4.1, TvAtg4.2, TvAtg4.3, TvAtg4.4, and TvAtg4.5). While transcription of *tvatg4.1,* followed by *tvatg4.4* seems to peak under GR conditions [16], translation of *tvatg4.4* into a protein was detected only under IR and HI conditions [19]. Here we identify TvAtg8a and TvAtg8b as substrates of TvAtg4.4 and describe rTvAtg4.4 autophagin *in vitro* activity by demonstrating by SDS-PAGE the release of GST and TvAtg8a or TvAtg8b, when using recombinant TvAtg8aGST or TvAtg8bGST as substrates [21]. *T. vaginalis* proteins TvAtg8a and TvAtg8b share 44% identity and, like many other organisms including *H. sapiens'* ATG8 contain the conserved Gly residue that is required for recognition by the TvAtg4.4 protease (Supplementary Figure S1).

Despite differences in secondary structure compared to the crystallized HsATG4B, TvAtg4.4 autophagin maintains the two main domains of the C54 family: i) the protease domain and its two distinct subdomains, containing the catalytic triad Cys^{52}/His^{216}/Asp^{214}. ii) The auxiliary domain formed by two α-helices (Figure 2). Reports on the crystal structure of HsATG4B show that it is self-inhibited by a cap loop formed by a GKPNSA motif and by Trp^{142}, which is close to the catalytic Cys. and is also involved in substrate recognition, as mutation of the residue results in protease activity loss. *In silico* analysis of TvAtg4.4 revealed similarities to HsATG4B, such as the cap loop and the conserved Trp^{116} (Figure 2B) [26,28]. Identifying the APEAR and cLIR motifs (Figure 2) at the *in silico* level in TvAtg4.4 suggests that there is a timely regulation in the autophagosome deconjugation of TvAtg8-PE by TvAtg4.4. Therefore, we propose that TvAtg4.4 autophagin follows the model already reported during the biogenesis of the autophagosome, where the LIR junction pocket is protected to avoid premature interaction between TvAtg4.4 and TvAtg8a/b in cytoplasm and in the inner membrane of the autophagosome, due to steric impediment and/or competition, avoiding association. In addition, the APEAR motif could allow specific recognition of the TvAtg8a/b-PE C-terminal for its autophagic membrane deconjugation [27,33,34]. Further experiments are needed to corroborate whether it also participates in the recognition of TvAtg8a or TvAtg8b (Figure 2C).

Having confirmed *in silico* that TvAtg4.4 has the canonical catalytic triad of the autophagin family, we evaluated whether the rTvAtg4.4 protease could process the recombinant substrates TvAtg8aGST and TvAtg8bGST. Increasing concentrations of rTvAtg4.4 with the rTvAtg8aGST substrate resulted in a linear digestion rate (Figure 4), which has been previously reported for other

 doi:10.20944/preprints202511.2032.v1

autophagins [35]. Under these conditions, no enzymatic activity was observed when using rTvAtg8bGST as substrate, even at high protease concentrations. This result was surprising and led us to search for enzyme hysteresis, where enzymes that can exhibit slow protease activity due to sudden changes in substrate ligand or activator, concentration, leading to the wrong conclusion that the protease is inactive. In these cases, it is suggested to increase protease interaction for extended periods, which could reveal the catalytic activity [36,37]. Thus, we tested the enzyme activity during increased interaction times with each substrate (Figure 5). rTvAtg4.4 showed higher *in vitro* enzymatic activity for TvAtg8aGST compared to TvAtg8bGST, requiring incubations of only 15 min for the former and 3 h for the latter. We therefore propose that rTvAtg4.4 displays enzymatic hysteresis towards TvAtg8bGST, assuming that TvAtg8bGST triggers a slow conformational change upon contact with the protease. The different enzymatic activities observed in rTvAtg4.4 with its two *T. vaginalis* substrates is consistent with reports of the activity of other ATG4s. For example, *H. sapiens* ATG4A can cleave the C-terminal end of all ATG8 isoforms; however, processing occurs at different times, ranging from 3 to 300 min [38].

Another explanation of the faster processing time of TvAtg8a vs. TvAtg8b could lay in the aa residue found before the C-terminal Gly. ATG4 requires the presence of Gly at the C-terminal end of ATG8 as mutations to Ala or its elimination results in the lack of enzymatic activity [39]. In addition, ATG4 shows higher specificity for its substrate when a Phe residue precedes the Gly, whereas any other aa residue decreases the specificity [38]. Interestingly, TvAtg8a does contain a Phe residue before the Gly, whereas TvAtg8b contains a Tyr residue (Supplementary Figure S1). Therefore, the differential behavior of TvAtg4.4 against TvAtg8a and TvAtg8b could be due to the difference between the aa residues prior to Gly. To corroborate this hypothesis, enzymatic activity after mutation assays on the Gly and Phe residues of both substrates need to be recorded.

Determining the kinetic parameters of an enzymatic reaction helps analyzing the affinity towards its substrate (Km) and the maximum reaction speed [Vmax]. A small Km value indicates high affinity of the protease to its substrate [40]. Here, we determined a Vmax value for TvAtg4.4 of 9.6 x 10^{-11} mM/s, while the Km value was 9.9 x 10^{-8} mM (9.9 x 10^{-6} mol/L) for TvAtg8a, which is comparable to HsATG4B Km of 5.1 x 10^{-6} mol/L for its substrates [37,38,41].

Proteases are grouped into families that share aa sequences; these, in turn, are classified into clans that share related tertiary structures [42]. TvAtg4.4 belongs to the CA Clan and to the C54 or autophagin family. The CA clan is represented by papain-like proteases, characterized by using a cysteine residue for the hydrolysis of the bond to be catalyzed, where the catalytic triad Cys/His/Asn (or Asp) is always involved [43]. We here report that TvAtg4.4 has the canonical catalytic triad (Cys^{52}/His^{216}/Asp^{214}) and that its activity depends on a cysteine residue through enzyme inhibition assays using protease inhibitors for the different *T. vaginalis* protease families [44–46]. The results presented in Figures 7A and B showed that the rTvAtg4.4 activity was almost entirely inhibited by IAM and partially by E-64. This result confirms, as with other autophagins, its catalytic activity depends on Cys^{52}, since IAM alkylates the thiol group of Cys, forming a covalent bond (S-carboxydomethylcysteine) [47]. Interestingly, partial inhibition of TvAtg4.4 activity was observed with E-64, a specific inhibitor of papain-like proteases that irreversibly binds to the thiol group of Cys. A complete inhibition of TvAtg4.4 catalytic activity was probably hindered by the closed cap loop near the active site, as identified in the *in silico* analysis (Figure 2C), which could prevent access of the large E-64 inhibitor, but not the small IAM molecule to the catalytic Cys^{52} [26,47,48]. Subsequent assays in which Cys^{52} is deleted from TvAtg4.4 will help demonstrate whether its protease activity is due to this residue, and not to any other four remaining Cys.

Exploring the substrate specificity of rTvAtg4.4 [49], we performed comparative assays using TvAtg8aGST or BSA, as substrates. Results corroborate the specificity of TvAtg4.4 for TvAtg8aGST (Figures 7C and D), which is consistent with previous observations that processing of the ATG8 family is carried out solely by the C54 proteases [50]. In addition, we corroborated this finding by FWB, which shows the direct binding of TvAtg4.4-TvAtg8aGST and TvAtg4.4-TvAtg8bGST (Figures 7E and F) [51].

 doi:10.20944/preprints202511.2032.v1

Since nutrient stress has been reported to trigger macroautophagy in *T. vaginalis* [16], we analyzed the effect of GR and HG culture conditions on TvAtg4.4 activity. Glucose is the primary source of carbon and energy of *T. vaginalis*; the parasite is exposed to different glucose levels during infection (0.3-36.65 mM) [52]. HG provides optimal metabolic conditions for cell division and the establishment of infection, whereas GR conditions derive in metabolic stress and activation of survival pathways such as autophagy, leading to improved antioxidant capacity [16]. In this work, we focused on analyzing the effect of different glucose conditions (GR and HG; ≤1 mM and 50 mM, respectively) on TvAtg4.4 transcription, translation, and enzymatic activity.

Results show that transcription of *tvatg4.4* is positively regulated under GR conditions. These results agree with those previously reported by Huang *et al*. (2019), who found that the different Atg4-type genomic sequences in *T. vaginalis* are positively regulated under GR conditions [16]. *In silico* analysis of the 5´ region of *tvatg4.4* showed basal transcription elements, but no typical glucose response elements (E-box) (Figure 2) [53]. An interesting challenge in the future will be to look for these regulatory sequences.

Translation analysis of TvAtg4.4, in WB assays using a polyclonal anti-rTvAtg4.4 antibody showed recognition of 5 bands (110, 45, 35, 27 and 22 kDa). Unlike other cysteine proteases, *T. vaginalis* autophagin, does not undergo proteolytic processing for its activation. Rather, its activation is substrate-dependent as in other autophagins. While the expected and calculated size of this protein is ~35 kDa, the observed ~45 and ~110 kDa bands could correspond to PTMs of the protein and the formation of oligomers, respectively. A regulatory mechanism of HsATG4B involves oxidation-reduction reactions, in which intra- and inter-molecular disulfide bridges form between Cys residues. Therefore, when using reducing agents (DTT), only one band should be observed. In contrast, oxidizing agents (H_2O_2) agent induced the formation of intramolecular bonds between Cys. Increasing the concentration of the oxidizing agent rises intermolecular bonds, leading to ATG4 oligomerization, the appearance of high-molecular-weight bands, and, ultimately, the loss of protease activity. Based on these observations, TvAtg4.4 high-molecular-weight bands could be due to low activity of the reducing agent (β-mercaptoethanol) compared to DTT [54–57]. Therefore, we could hypothesize around a spatiotemporal regulation of TvAtg4.4 protease activity through the formation of some ~110 kDa and higher molecular weight oligomers that could be modulated by the presence of glucose. Degradation of the TvAtg4.4 autophagin could explain the ~27 and ~22 kDa bands (Figure 8), supported by their lysosomal localization (Figure 12).

In other eukaryotes, ATG4 participates in two ATG8 processing steps, namely in the initiation of autophagy through the processing of newly synthesized ATG8 family proteins, and in the removal of ATG8 from the outer membrane of the autophagosome prior to lysosome-autophagosome fusion [32–34,58,59]. This suggests that the autophagin family is localized in the cytoplasm and the ER. In our study, TvAtg4.4 was found in cytoplasm and ER, as other autophagins. In addition, TvAtg4.4 was also found in other compartments, V, AV, G, N, and H. IFA confirmed that TvAtg4.4 localized in autophagic vesicles (Figure 9), as revealed by its colocalization with the autophagy markers TvAtg8a and TvAtg8b, previously reported in *T. vaginalis* [17,18]. However, some vesicles containing TvAtg4.4 (green) did not have autophagy markers; instead, colocalized in lysosomes using lysotracker as a marker. Thus, we also demonstrated the lysosomal origin of these vesicles (Figure 12). The presence of low-molecular-weight bands by WB (~27 and ~22 kDa) (Figure 8) suggest that TvAtg4.4 could be directed into the endolysosomal system for degradation [59,60].

In addition, immuno-gold-TEM images suggested the presence of TvAtg4.4 in hydrogenosomes. Using PFOa as a marker of hydrogenosomes [25,61,62], we confirmed by IFA colocalization with TvAtg4.4 (Figure 13). There are no reports on the presence of autophagins in hydrogenosomes. We present different hypotheses to explain this observation. i) Hydrogenosomal sequestration per se will avoid the cytoplasmic TvAtg4.4 enzymatic activity. ii) Since a regulatory mechanism for these proteins involves redox reactions that render them inactive, the hydrogenosome oxidative environment [62,63] may serve as a regulatory mechanism for TvAtg4.4 activation or deactivation by forming oligomers. iii) The presence of autophagic proteins such as TvAtg4.4 in hydrogenosomes

 doi:10.20944/preprints202511.2032.v1

could serve as a marker for a non-canonical secretory autophagy for PFOa via hydrogenophagy [25; unpublished data]. However, additional studies are needed to demonstrate this and to understand TvAtg4.4 association with hydrogenosomes in *T. vaginalis*.

5. Conclusions

In conclusion, the results obtained in this work indicate that TvAtg4.4 is a *T. vaginalis* active autophagin, capable of *in vitro* processing of the autophagosome markers TvAtg8a and TvAtg8b. This suggests that *T. vaginalis* displays a macroautophagic process similar to the one observed in higher eukaryotes, that involves TvAtg4.4 autophagin and its substrates, TvAtg8a and TvAtg8b.

Supplementary Materials: The following supporting information can be downloaded at the website of this paper posted on Preprints.org. Figure S1: Multiple alignment of aa sequences of ATG8 proteins; Figure S2: Purification of recombinant proteins TvAtg4.4, TvAtg8aGST, and TvAtg8bGST; Figure S3: Western blot analysis of products released from the TvAtg4.4-TvAtg8aGST and TvAtg4.4–TvAtg8bGST enzyme assays; Figure S4: Purification of recombinant GST protein for a calibration curve.

Author Contributions: Conceptualization, R.A. and M.G.M.C.; methodology, M.G.M.C., C.I.F.P., and L.I.S.V.; validation, R.A., M.G.M.C., L.I.S.V., M.E.C., C.I.F.P., and J.O.L.; formal analysis, R.A., M.G.M.C., L.I.S.V.; C.I.F.P., and J.O.L.; investigation, R.A., M.G.M.C., and J.O.L.; resources, R.A.; data curation, R.A., M.G.M.C., L.I.S.V.; M.E.C., C.I.F.P., and J.O.L.; writing—original draft preparation, M.G.M.C.; writing—review and editing, M.G.M.C., M.E.C., and R.A.; visualization, R.A., M.G.M.C., L.I.S.V.; M.E.C., and J.O.L.; supervision, R.A., C.I.F.P., and J.O.L.; project administration, R.A.; funding acquisition, R.A., and J.O.L. All authors have read and agreed to the published version of the manuscript.

Funding: This research was funded by Grant 074 SEP-CINVESTAV (to R.A.), "UNESCO-Equatorial Guinea International Prize for Research in Life Sciences 2012" (to R.A.), "Premio para las Mujeres en la Ciencia L'Oreal-UNESCO-AMC-CONALMEX 2023" (to R.A.), "Premio Ada Byron 2025 para la Mujer Tecnóloga" (to R.A.), and grant INFRA-2016 269657 (to J.O.L.) from CONACYT, México.

Institutional Review Board Statement: The study was conducted in accordance with the Declaration of Helsinki and approved by the Institutional Review Board CICUAL for antibody production in mice and rabbits (Protocol 0229-16); approval date: 08/16/2022.

Informed Consent Statement: Not applicable.

Data Availability Statement: The data presented in this study are available on request from the corresponding author.

Acknowledgments: We thank MVZ. Jorge Octavio Ramos Flores for his help in handling rabbits to produce polyclonal antibodies. We also thank QFB Leticia Avila Gonzalez and Oscar Vargas for producing mice polyclonal antibodies and to PhD Veronica Aranda-Chan for her kind donation of the recombinant Chagasin protein. We thank Dr. Fidel de la Cruz Hernández-Hernández and Leticia Cortés-Martínez for their support in performing qPCR and Martha G. Aguilar-Romero for her secretarial assistance. This work is the scientific project of Miriam Guadalupe Mateo Cruz to obtain her Ph.D. degree in Infectómica y Patogénesis Molecular (DIPM-Cinvestav). She was supported by a Ph.D. scholarship (1002671) from CONACYT, Mexico.

Conflicts of Interest: The authors declare no conflicts of interest.

References

1. Aman, Y., Schmauck-Medina, T., Hansen, M., Morimoto, R. I., Simon, A. K., Bjedov, I., Palikaras, K., Simonsen, A., Johansen, T., Tavernarakis, N., Rubinsztein, D. C., Partridge, L., Kroemer, G., Labbadia, J., & Fang, E. F. (2021). Autophagy in healthy aging and disease. *Nature Aging*, *1*(8), 634–650. https://doi.org/10.1038/s43587-021-00098-4
2. Dikic, I., & Elazar, Z. (2018). Mechanism and medical implications of mammalian autophagy. *Nature Reviews. Molecular Cell Biology*, *19*(6), 349–364. https://doi.org/10.1038/s41580-018-0003-4

 doi:10.20944/preprints202511.2032.v1

3. Chang N. C. (2020). Autophagy and stem cells: Self-eating for self-renewal. *Frontiers in Cell and Developmental Biology*, *8*, 138. https://doi.org/10.3389/fcell.2020.00138
4. Yin, Z., Pascual, C., & Klionsky, D. J. (2016). Autophagy: machinery and regulation. *Microbial Cell (Graz, Austria)*, *3*(12), 588–596. https://doi.org/10.15698/mic2016.12.546
5. Yu, L., Chen, Y., & Tooze, S. A. (2018). Autophagy pathway: Cellular and molecular mechanisms. *Autophagy*, *14*(2), 207–215. https://doi.org/10.1080/15548627.2017.1378838
6. Li, X., He, S., & Ma, B. (2020). Autophagy and autophagy-related proteins in cancer. *Molecular Cancer*, *19*(1), 12. https://doi.org/10.1186/s12943-020-1138-4
7. Noda, N. N., Ohsumi, Y., & Inagaki, F. (2009). ATG systems from the protein structural point of view. *Chemical Reviews*, *109*(4), 1587–1598. https://doi.org/10.1021/cr800459r
8. Xie, Z., & Klionsky, D. J. (2007). Autophagosome formation: core machinery and adaptations. *Nature Cell Biology*, *9*(10), 1102–1109. https://doi.org/10.1038/ncb1007-1102
9. Mizushima N. (2020). The ATG conjugation systems in autophagy. *Current Opinion in Cell Biology*, *63*, 1–10. https://doi.org/10.1016/j.ceb.2019.12.001
10. Martens, S., & Fracchiolla, D. (2020). Activation and targeting of ATG8 protein lipidation. *Cell Discovery*, *6*, 23. https://doi.org/10.1038/s41421-020-0155-1
11. Glick, D., Barth, S., & Macleod, K. F. (2010). Autophagy: cellular and molecular mechanisms. *The Journal of Pathology*, *221*(1), 3–12. https://doi.org/10.1002/path.2697
12. Centers for Disease Control and Prevention. (CDC). About trichomoniasis. Retrieved October 22, 2025, from https://www.cdc.gov/trichomoniasis/es/about/acerca-de-la-tricomoniasis.html
13. Edwards, T., Burke, P., Smalley, H., & Hobbs, G. (2016). *Trichomonas vaginalis*: Clinical relevance, pathogenicity and diagnosis. *Critical Reviews in Microbiology*, *42*(3), 406–417. https://doi.org/10.3109/1040841X.2014.958050
14. Poole, D. N., & McClelland, R. S. (2013). Global epidemiology of *Trichomonas vaginalis*. *Sexually Transmitted Infections*, *89*(6), 418–422. https://doi.org/10.1136/sextrans-2013-051075
15. Kissinger P. (2015). *Trichomonas vaginalis*: a review of epidemiologic, clinical and treatment issues. *BMC Infectious Diseases*, *15*, 307. https://doi.org/10.1186/s12879-015-1055-0
16. Huang, K. Y., Chen, Y. Y., Fang, Y. K., Cheng, W. H., Cheng, C. C., Chen, Y. C., Wu, T. E., Ku, F. M., Chen, S. C., Lin, R., & Tang, P. (2014). Adaptive responses to glucose restriction enhance cell survival, antioxidant capability, and autophagy of the protozoan parasite *Trichomonas vaginalis*. *Biochimica et Biophysica Acta*, 1840(1), 53–64. https://doi.org/10.1016/j.bbagen.2013.08.008
17. Huang, K. Y., Chen, R. M., Lin, H. C., Cheng, W. H., Lin, H. A., Lin, W. N., Huang, P. J., Chiu, C. H., & Tang, P. (2019). Potential role of autophagy in proteolysis in Trichomonas vaginalis. *Journal of Microbiology, Immunology, and Infection* = Wei mian yu gan ran za zhi, 52(2), 336–344. https://doi.org/10.1016/j.jmii.2018.11.002
18. Hernández-García, M. S., Miranda-Ozuna, J. F. T., Salazar-Villatoro, L., Vázquez-Calzada, C., Ávila-González, L., González-Robles, A., Ortega-López, J., & Arroyo, R. (2019). Biogenesis of autophagosome in *Trichomonas vaginalis* during macroautophagy induced by rapamycin-treatment and iron or glucose starvation conditions. *The Journal of Eukaryotic Microbiology*, 66(4), 654–669. https://doi.org/10.1111/jeu.12712
19. Dias-Lopes, G., Wiśniewski, J. R., de Souza, N. P., Vidal, V. E., Padrón, G., Britto, C., Cuervo, P., & De Jesus, J. B. (2018). In-depth quantitative proteomic analysis of trophozoites and pseudocysts of *Trichomonas vaginalis*. *Journal of Proteome Research*, *17*(11), 3704–3718. https://doi.org/10.1021/acs.jproteome.8b00343
20. Goulas, T., Cuppari, A., Garcia-Castellanos, R., Snipas, S., Glockshuber, R., Arolas, J. L., & Gomis-Rüth, F. X. (2014). The pCri system: a vector collection for recombinant protein expression and purification. *PloS One*, *9*(11), e112643. https://doi.org/10.1371/journal.pone.0112643.
21. Li, M., Fu, Y., Yang, Z., & Yin, X. M. (2017). Measurement of the activity of the Atg4 cysteine proteases. *Methods in Enzymology*, 587, 207–225. https://doi.org/10.1016/bs.mie.2016.10.024
22. Cárdenas-Guerra, R. E., Montes-Flores, O., Nava-Pintor, E. E., Resendiz-Cardiel, G., Flores-Pucheta, C. I., Rodriguez-Gavaldon, Y. I., Arroyo, R., Bottazzi, M. E., Hotez, P. J., and Ortega-Lopez, J. (**2024**) Chagasin

 doi:10.20944/preprints202511.2032.v1

from Trypanosoma cruzi as a molecular scaffold to express epitopes of TSA-1 as soluble recombinant chimeras, *Protein Expr Purif 218*, 106458.

23. Dos Santos, O., de Vargas Rigo, G., Frasson, A. P., Macedo, A. J., & Tasca, T. (2015). Optimal reference genes for gene expression normalization in *Trichomonas vaginalis*. *PloS One*, *10*(9), e0138331. https://doi.org/10.1371/journal.pone.0138331
24. Euceda-Padilla, E. A., Mateo-Cruz, M. G., Ávila-González, L., Flores-Pucheta, C. I., Ortega-López, J., Talamás-Lara, D., Velazquez-Valassi, B., Jasso-Villazul, L., & Arroyo, R. (2024). *Trichomonas vaginalis* legumain-2, TvLEGU-2, is an immunogenic cysteine peptidase expressed during trichomonal infection. *Pathogens (Basel, Switzerland)*, *13*(2), 119. https://doi.org/10.3390/pathogens13020119
25. Meza-Cervantez, P., González-Robles, A., Cárdenas-Guerra, R. E., Ortega-López, J., Saavedra, E., Pineda, E., & Arroyo, R. (2011). Pyruvate:ferredoxin oxidoreductase (PFO) is a surface-associated cell-binding protein in *Trichomonas vaginalis* and is involved in trichomonal adherence to host cells. *Microbiology (Reading, England)*, *157*(Pt 12), 3469–3482. https://doi.org/10.1099/mic.0.053033-0
26. Kumanomidou, T., Mizushima, T., Komatsu, M., Suzuki, A., Tanida, I., Sou, Y. S., Ueno, T., Kominami, E., Tanaka, K., & Yamane, T. (2006). The crystal structure of human Atg4b, a processing and de-conjugating enzyme for autophagosome-forming modifiers. *Journal of Molecular Biology*, *355*(4), 612–618. https://doi.org/10.1016/j.jmb.2005.11.018
27. Rogov, V. V., Nezis, I. P., Tsapras, P., Zhang, H., Dagdas, Y., Noda, N. N., Nakatogawa, H., Wirth, M., Mouilleron, S., McEwan, D. G., Behrends, C., Deretic, V., Elazar, Z., Tooze, S. A., Dikic, I., Lamark, T., & Johansen, T. (2023). Atg8 family proteins, LIR/AIM motifs and other interaction modes. *Autophagy Reports*, *2*(1), 2188523. https://doi.org/10.1080/27694127.2023.2188523
28. Satoo, K., Suzuki, N. N., Fujioka, Y., Mizushima, N., Ohsumi, Y., & Inagaki, F. (2007). Crystallization and preliminary crystallographic analysis of human Atg4B-LC3 complex. *Acta crystallographica. Section F, Structural biology and crystallization communications*, *63*(Pt 2), 99–102. https://doi.org/10.1107/S1744309106056429
29. Liston, D. R., & Johnson, P. J. (1999). Analysis of a ubiquitous promoter element in a primitive eukaryote: early evolution of the initiator element. *Molecular and Cellular Biology*, *19*(3), 2380–2388. https://doi.org/10.1128/MCB.19.3.2380
30. Smith, A. J., Chudnovsky, L., Simoes-Barbosa, A., Delgadillo-Correa, M. G., Jonsson, Z. O., Wohlschlegel, J. A., & Johnson, P. J. (2011). Novel core promoter elements and a cognate transcription factor in the divergent unicellular eukaryote *Trichomonas vaginalis*. *Molecular and Cellular Biology*, *31*(7), 1444–1458. https://doi.org/10.1128/MCB.00745-10
31. Espinosa, N., Hernández, R., López-Griego, L., & López-Villaseñor, I. (2002). Separable putative polyadenylation and cleavage motifs in *Trichomonas vaginalis* mRNAs. *Gene*, *289*(1-2), 81–86. https://doi.org/10.1016/s0378-1119(02)00476-6.
32. Kirisako, T., Ichimura, Y., Okada, H., Kabeya, Y., Mizushima, N., Yoshimori, T., Ohsumi, M., Takao, T., Noda, T., & Ohsumi, Y. (2000). The reversible modification regulates the membrane-binding state of Apg8/Aut7 essential for autophagy and the cytoplasm to vacuole targeting pathway. *The Journal of Cell Biology*, *151*(2), 263–276. https://doi.org/10.1083/jcb.151.2.263
33. Hirata, E., Ohya, Y., & Suzuki, K. (2017). Atg4 plays an important role in efficient expansion of autophagic isolation membranes by cleaving lipidated Atg8 in *Saccharomyces cerevisiae*. *Plos One*, *12 (7)*, e0181047. https://doi.org/10.1371/journal.pone.0181047
34. Zhou, Y., Wang, Z., Huang, Y., Bai, C., Zhang, X., Fang, M., Ju, Z., & Liu, B. (2022). Membrane dynamics of ATG4B and LC3 in autophagosome formation. *Journal of Molecular Cell Biology*, *13*(12), 853–863. https://doi.org/10.1093/jmcb/mjab059
35. Abreu, S., Kriegenburg, F., Gómez-Sánchez, R., Mari, M., Sánchez-Wandelmer, J., Skytte Rasmussen, M., Soares Guimarães, R., Zens, B., Schuschnig, M., Hardenberg, R., Peter, M., Johansen, T., Kraft, C., Martens, S., & Reggiori, F. (2017). Conserved Atg8 recognition sites mediate Atg4 association with autophagosomal membranes and Atg8 deconjugation. *EMBO Reports*, *18*(5), 765–780. https://doi.org/10.15252/embr.201643146

 doi:10.20944/preprints202511.2032.v1

36. Robinson P. K. (2015). Enzymes: principles and biotechnological applications. *Essays in Biochemistry*, *59*, 1–41. https://doi.org/10.1042/bse0590001
37. Rendón, J. L., & Pardo, J. P. (2025). Time-dependent kinetic complexities in enzyme assays: A review. *Biomolecules*, *15*(5), 641. https://doi.org/10.3390/biom15050641
38. Li, M., Hou, Y., Wang, J., Chen, X., Shao, Z. M., & Yin, X. M. (2011). Kinetics comparisons of mammalian Atg4 homologues indicate selective preferences toward diverse Atg8 substrates. *The Journal of Biological Chemistry*, *286*(9), 7327–7338. https://doi.org/10.1074/jbc.M110.199059
39. Shu, C. W., Drag, M., Bekes, M., Zhai, D., Salvesen, G. S., & Reed, J. C. (2010). Synthetic substrates for measuring activity of autophagy proteases: autophagins (Atg4). *Autophagy*, *6*(7), 936–947. https://doi.org/10.4161/auto.6.7.13075
40. Tanida, I., Sou, Y. S., Minematsu-Ikeguchi, N., Ueno, T., & Kominami, E. (2006). Atg8L/Apg8L is the fourth mammalian modifier of mammalian Atg8 conjugation mediated by human Atg4B, Atg7 and Atg3. *The FEBS Journal*, *273*(11), 2553–2562. https://doi.org/10.1111/j.1742-4658.2006.05260.x
41. Silverstein T. P. (2019). When both Km and Vmax are altered, Is the enzyme inhibited or activated? *Biochemistry and Molecular Biology Education: a bimonthly publication of the International Union of Biochemistry and Molecular Biology*, *47*(4), 446–449. https://doi.org/10.1002/bmb.21235
42. Rajković, J., Poreba, M., Caglič, D., Vidmar, R., Wilk, A., Borowik, A., Salvesen, G., Turk, V., Drag, M., & Turk, B. (2015). Biochemical characterization and substrate specificity of autophagin-2 from the parasite *Trypanosoma cruzi*. *The Journal of Biological Chemistry*, *290*(47), 28231–28244. https://doi.org/10.1074/jbc.M115.687764
43. Rawlings, N. D., Barrett, A. J., Thomas, P. D., Huang, X., Bateman, A., & Finn, R. D. (2018). The MEROPS database of proteolytic enzymes, their substrates and inhibitors in 2017 and a comparison with peptidases in the PANTHER database. *Nucleic Acids Research*, *46*(D1), D624–D632. https://doi.org/10.1093/nar/gkx1134
44. Yang, N., Matthew, M. A., & Yao, C. (2023). Roles of cysteine proteases in biology and pathogenesis of parasites. *Microorganisms*, *11*(6), 1397. https://doi.org/10.3390/microorganisms11061397
45. Hernández-Gutiérrez, R., Avila-González, L., Ortega-López, J., Cruz-Talonia, F., Gómez-Gutierrez, G., & Arroyo, R. (2004). *Trichomonas vaginalis*: characterization of a 39-kDa cysteine proteinase found in patient vaginal secretions. *Experimental Parasitology*, *107*(3-4), 125–135. https://doi.org/10.1016/j.exppara.2004.05.004
46. Mancilla-Olea, M. I., Ortega-López, J., Figueroa-Angulo, E. E., Avila-González, L., Cárdenas-Guerra, R. E., Miranda-Ozuna, J. F. T., González-Robles, A., Hernández-García, M. S., Sánchez-Ayala, L., & Arroyo, R. (2018). *Trichomonas vaginalis* cathepsin D-like aspartic proteinase (Tv-CatD) is positively regulated by glucose and degrades human hemoglobin. *The International Journal of Biochemistry & Cell Biology*, *97*, 1–15. https://doi.org/10.1016/j.biocel.2018.01.015
47. Grant G. A. (2017). Modification of cysteine. *Current Protocols in Protein Science*, *87*, 15.1.1–15.1.23. https://doi.org/10.1002/cpps.22
48. Matsumoto, K., Mizoue, K., Kitamura, K., Tse, W. C., Huber, C. P., & Ishida, T. (1999). Structural basis of inhibition of cysteine proteases by E-64 and its derivatives. *Biopolymers*, *51*(1), 99–107. https://doi.org/10.1002/(SICI)1097-0282(1999)51:1<99::AID-BIP11>3.0.CO; 2-R
49. Liu, W. L., Wen, Z. H., Li, Q. Y., Liu, H. B., Li, Q. L., Deng, S. Z., Zeng, Z. Y., Luo, M. C., Tang, A. X., & Liu, Y. Y. (2025). New insights into exploring new functional enzymes through the enzyme promiscuity. *International Journal of Biological Macromolecules*, *304*(Pt 1), 140576. https://doi.org/10.1016/j.ijbiomac.2025.140576
50. Zhang, L., Li, J., Ouyang, L., Liu, B., & Cheng, Y. (2016). Unraveling the roles of Atg4 proteases from autophagy modulation to targeted cancer therapy. *Cancer Letters*, *373*(1), 19–26. https://doi.org/10.1016/j.canlet.2016.01.022
51. Wu, Y., Li, Q., & Chen, X. Z. (2007). Detecting protein-protein interactions by Far western blotting. *Nature Protocols*, *2*(12), 3278–3284. https://doi.org/10.1038/nprot.2007.459
52. Miranda-Ozuna, J. F., Hernández-García, M. S., Brieba, L. G., Benítez-Cardoza, C. G., Ortega-López, J., González-Robles, A., & Arroyo, R. (2016). The glycolytic enzyme triosephosphate isomerase of *Trichomonas*

 doi:10.20944/preprints202511.2032.v1

vaginalis is a surface-associated protein induced by glucose that functions as a laminin- and fibronectin-binding protein. *Infection and Immunity*, *84*(10), 2878–2894. https://doi.org/10.1128/IAI.00538-16

53. Vaulont, S., Vasseur-Cognet, M., & Kahn, A. (2000). Glucose regulation of gene transcription. *The Journal of Biological Chemistry*, *275*(41), 31555–31558. https://doi.org/10.1074/jbc.R000016200
54. Zheng, X., Yang, Z., Gu, Q., Xia, F., Fu, Y., Liu, P., Yin, X. M., & Li, M. (2020). The protease activity of human ATG4B is regulated by reversible oxidative modification. *Autophagy*, *16*(10), 1838–1850. https://doi.org/10.1080/15548627.2019.1709763
55. Pérez-Pérez, M. E., Lemaire, S. D., & Crespo, J. L. (2021). The ATG4 protease integrates redox and stress signals to regulate autophagy. *Journal of Experimental Botany*, *72*(9), 3340–3351. https://doi.org/10.1093/jxb/erab063
56. Pérez-Pérez, M. E., Zaffagnini, M., Marchand, C. H., Crespo, J. L., & Lemaire, S. D. (2014). The yeast autophagy protease Atg4 is regulated by thioredoxin. *Autophagy*, *10*(11), 1953–1964. https://doi.org/10.4161/auto.34396
57. Cleland W. W. (1964). Dithiothreitol, a new protective reagent for SH groups. *Biochemistry*, *3*, 480–482. https://doi.org/10.1021/bi00892a002
58. Xie, Z., Nair, U., & Klionsky, D. J. (2008). Atg8 controls phagophore expansion during autophagosome formation. *Molecular Biology of the Cell*, *19*(8), 3290–3298. https://doi.org/10.1091/mbc.e07-12-1292
59. Fujita, N., Hayashi-Nishino, M., Fukumoto, H., Omori, H., Yamamoto, A., Noda, T., & Yoshimori, T. (2008). An Atg4B mutant hampers the lipidation of LC3 paralogues and causes defects in autophagosome closure. *Molecular Biology of the Cell*, *19*(11), 4651–4659. https://doi.org/10.1091/mbc.e08-03-0312
60. Luzio, J. P., Pryor, P. R., & Bright, N. A. (2007). Lysosomes: fusion and function. *Nature Reviews. Molecular Cell Biology*, *8*(8), 622–632. https://doi.org/10.1038/nrm2217
61. Schneider, R. E., Brown, M. T., Shiflett, A. M., Dyall, S. D., Hayes, R. D., Xie, Y., Loo, J. A., & Johnson, P. J. (2011). The *Trichomonas vaginalis* hydrogenosome proteome is highly reduced relative to mitochondria, yet complex compared with mitosomes. *International Journal for Parasitology*, *41*(13-14), 1421–1434. https://doi.org/10.1016/j.ijpara.2011.10.001
62. Embley, T. M., van der Giezen, M., Horner, D. S., Dyal, P. L., & Foster, P. (2003). Mitochondria and hydrogenosomes are two forms of the same fundamental organelle. *Philosophical Transactions of the Royal Society of London. Series B, Biological Sciences*, *358*(1429), 191–202. https://doi.org/10.1098/rstb.2002.1190
63. Smutná, T., Dohnálková, A., Sutak, R., Narayanasamy, R. K., Tachezy, J., & Hrdý, I. (2022). A cytosolic ferredoxin-independent hydrogenase possibly mediates hydrogen uptake in *Trichomonas vaginalis*. *Current Biology: CB*, *32*(1), 124–135.e5. https://doi.org/10.1016/j.cub.2021.10.050